

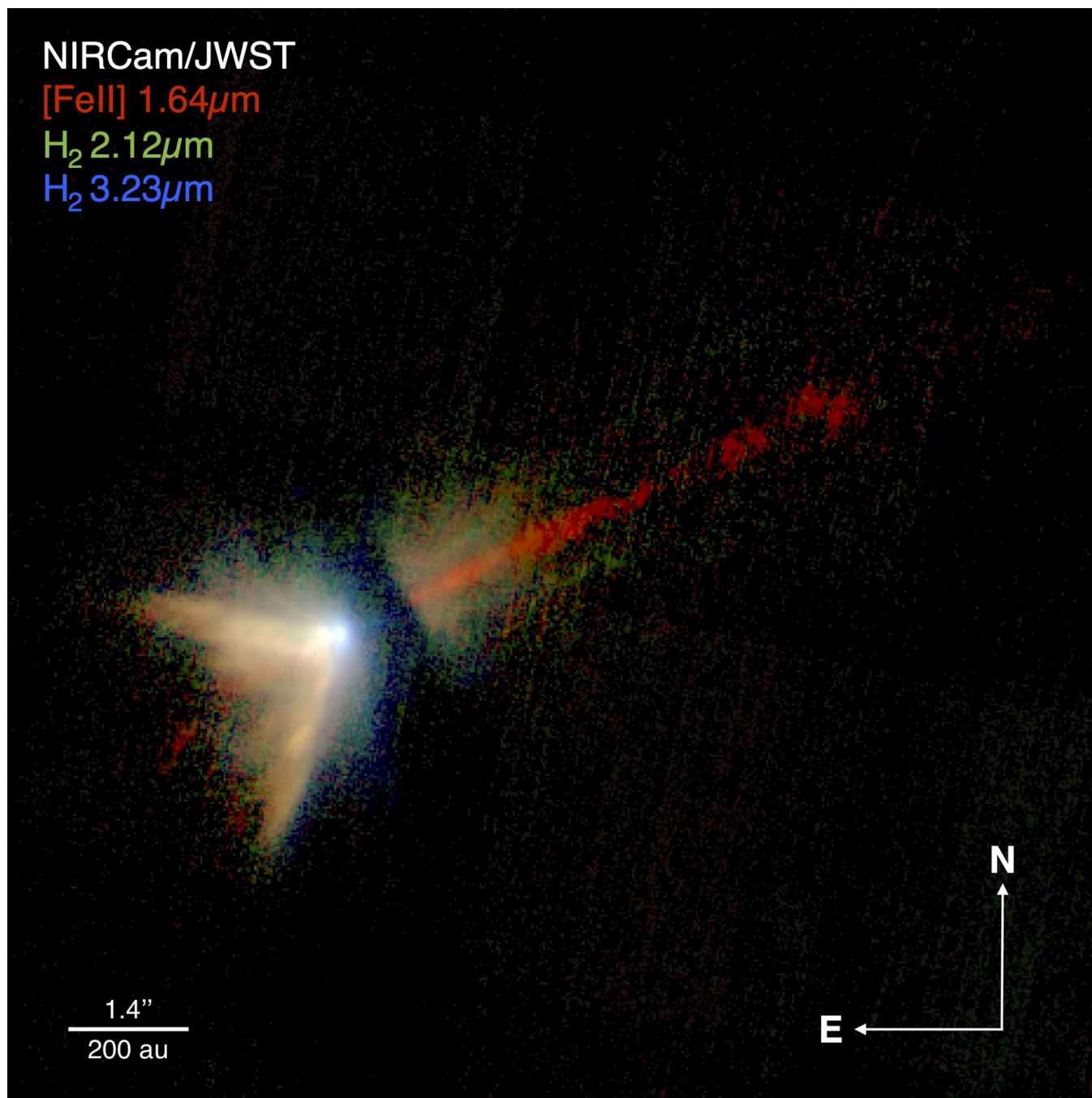
# The Star Formation Newsletter

A community newsletter on Star and Planet Formation research

No. 374 — 29 Feb 2024

Editor: João Alves

[www.starformation.news](http://www.starformation.news)



## Cover image caption

RGB image of DG Tau B combining three NIRCам exposures in F164N (red) for the [FeII] 1.64 $\mu$ m line + continuum, F212N (green) for the H2 1-0S(1) 2.12 $\mu$ m line + continuum, and F323N (blue) for the 1-0O(5) 3.23 $\mu$ m line + continuum.

Credits: NASA, ESA, CSA, STScI, Delabrosse et al. 2024

## Note from the Editor

The Star Formation Newsletter is now on the web at [www.starformation.news](http://www.starformation.news). This PDF file contains the monthly Abstracts and links. Red text in this PDF is a url link. Submitting an abstract to the SFN is as simple as entering the arXiv ID (e.g., 2006.10139) in a [web form](#) on the SFN web site. **Do not remove the L<sup>A</sup>T<sub>E</sub>X formatting when submitting to the arXiv**. If you do, your abstract will not look great either at the arXiv or the SFN.

## Abstracts

### 1. **A Unified Model for Bipolar Outflows from Young Stars: Kinematic and Mixing Structures in HH 30**

Tsung-Han Ai, Chun-Fan Liu, Hsien Shang, Doug Johnstone, Ruben Krasnopolsky ★ The young stellar source HH 30 is a textbook example of an ionic optical jet originating from a disk in an edge-on system shown by the HST. It has a remnant envelope in <sup>12</sup>CO observed by ALMA. The optical jet is characterized by its narrow appearance, large line width at the base, and high temperature inferred from line diagnostics. Three featured structures can be identified, most evident in the transverse position–velocity diagrams: an extremely–high–velocity (EHV) wide-angle wind component with large spectral widths in the optical, a very–low–velocity (VLV) ambient surrounding medium seen in <sup>12</sup>CO, and a low-velocity (LV) region traced by <sup>12</sup>CO nested both in velocity and location between the primary wind and ambient environment. A layered cavity with multiple shells forms nested morphological and kinematic structures around the optical jet. The atomic gas originating from the innermost region of the disk attains a sufficient temperature and ionization to emit brightly in forbidden lines as an optical jet. The wide-angle portion expands, forming a low-density cavity. The filamentary <sup>12</sup>CO encompassing the wind cavity is mixed and advected inward through the action of the magnetic interplay of the wide-angle wind with the molecular ambient medium. The magnetic interplay results in the layered shells penetrating deeply into the vast cavity of tenuous atomic wind material. The HH 30 system is an ideal manifestation of the unified wind model of Shang 2020,2023, with clearly distinguishable atomic and molecular species mixed through the atomic lightly ionized magnetized wind and the surrounding cold molecular ambient material.

### 2. **Evolution of the relation between the mass accretion rate and the stellar and disk mass from brown dwarfs to stars**

V. Almendros-Abad, C. F. Manara, L. Testi, A. Natta, R. A. B. Claes, K. Muzic, E. Sanchis, J. M. Alcalá, A. Bayo, A. Scholz ★ The time evolution of the dependence of the mass accretion rate with the stellar mass and the disk mass represents a fundamental way to understand the evolution of protoplanetary disks and the formation of planets. In this work, we present observations with X-Shooter of 26 Class II very low-mass stars and brown dwarfs in the Ophiuchus, Cha-I, and Upper Scorpius star-forming regions (SFRs). These new observations extend down to SpT M9 ( $\sim 0.02 M_{\odot}$ ) the measurement of the mass accretion rate in Ophiuchus and Cha-I and add 11 very-low-mass stars to the sample of objects studied with broadband spectroscopy in Upper Scorpius. We obtained their SpT, extinction and physical parameters, and we used the intensity of various emission lines to derive their accretion luminosity and mass accretion rates. Combining these new observations with data from the literature, we compare relations between accretion and stellar and disk properties of four different SFRs with different ages: Ophiuchus (1 Myr), Lupus (2 Myr), Cha-I (3 Myr), and Upper Scorpius (5-12 Myr). We find the slopes of the  $L_{*} - L_{\text{acc}}$  and  $M_{*} - \dot{M}_{\text{acc}}$  relationships to steepen between Ophiuchus, Lupus, and Cha-I and that both relationships may be better described with a single power law. We also find the relationship between the disk mass and the mass accretion rate of the stellar population to steepen with time down to the age of Upper Scorpius. Overall, we observe hints of a faster evolution into low accretion rates of low-mass stars and brown dwarfs. We also find that brown dwarfs present higher  $\dot{M}_{\text{disk}}/\dot{M}_{\text{acc}}$  ratios

(i.e., longer accretion depletion timescales) than stars in Ophiuchus, Lupus, and Cha-I. This apparently contradictory result may imply that the evolution of protoplanetary disks around brown dwarfs is different from what is seen in the stellar regime.

### 3. JWST MIRI MRS Images Disk Winds, Water, and CO in an Edge-On Protoplanetary Disk

Nicole Arulanantham, M. K. McClure, Klaus Pontoppidan, Tracy L. Beck, J. A. Sturm, D. Harsono, A. C. A. Boogert, M. Cordiner, E. Dartois, M. N. Drozdovskaya, C. Espaillat, G. J. Melnick, J. A. Noble, M. E. Palumbo, Y. J. Pendleton, H. Terada, E. F. van Dishoeck ★ We present JWST MIRI MRS observations of the edge-on protoplanetary disk around the young sub-solar mass star Tau 042021, acquired as part of the Cycle 1 GO program "Mapping Inclined Disk Astrochemical Signatures (MIDAS)." These data resolve the mid-IR spatial distributions of H<sub>2</sub>, revealing X-shaped emission extending to 200 au above the disk midplane with a semi-opening angle of  $35 \pm 5$  degrees. We do not velocity-resolve the gas in the spectral images, but the measured semi-opening angle of the H<sub>2</sub> is consistent with an MHD wind origin. A collimated, bipolar jet is seen in forbidden emission lines from [Ne II], [Ne III], [Ni II], [Fe II], [Ar II], and [S III]. Extended H<sub>2</sub>O and CO emission lines are also detected, reaching diameters between 90 and 190 au, respectively. Hot molecular emission is not expected at such radii, and we interpret its extended spatial distribution as scattering of inner disk molecular emission by dust grains in the outer disk surface. H I recombination lines, characteristic of inner disk accretion shocks, are similarly extended, and are likely also scattered light from the innermost star-disk interface. Finally, we detect extended PAH emission at 11.3 microns co-spatial with the scattered light continuum, making this the first low-mass T Tauri star around which extended PAHs have been confirmed, to our knowledge. MIRI MRS line images of edge-on disks provide an unprecedented window into the outflow, accretion, and scattering processes within protoplanetary disks, allowing us to constrain the disk lifetimes and accretion and mass loss mechanisms.

### 4. An ALMA molecular inventory of warm Herbig Ae disks: I. Molecular rings, asymmetries and complexity in the HD 100546 disk

Alice S. Booth, Margot Leemker, Ewine F. van Dishoeck, Lucy Evans, John D. Ilee, Mihkel Kama, Luke Keyte, Charles J. Law, Nienke van der Marel, Hideko Nomura, Shota Notsu, Karin Öberg, Milou Temmink, Catherine Walsh ★ Observations of disks with the Atacama Large Millimeter/submillimeter Array (ALMA) allow us to map the chemical makeup of nearby protoplanetary disks with unprecedented spatial resolution and sensitivity. The typical outer Class II disk observed with ALMA is one with an elevated C/O ratio and a lack of oxygen-bearing complex organic molecules, but there are now some interesting exceptions: three transition disks around Herbig Ae stars all show oxygen-rich gas traced via the unique detections of the molecules SO and CH<sub>3</sub>OH. We present the first results of an ALMA line survey at 337 to 357 GHz of such disks and focus this paper on the first Herbig Ae disk to exhibit this chemical signature - HD 100546. In these data, we detect 19 different molecules including NO, SO and CH<sub>3</sub>OCHO (methyl formate). We also make the first tentative detections of H<sub>2</sub>13CO and 34SO in protoplanetary disks. Multiple molecular species are detected in rings, which are, surprisingly, all peaking just beyond the underlying millimeter continuum ring at 200 au. This result demonstrates a clear connection between the large dust distribution and the chemistry in this flat outer disk. We discuss the physical and/or chemical origin of these sub-structures in relation to ongoing planet formation in the HD 100546 disk. We also investigate how similar and/or different the molecular makeup of this disk is to other chemically well-characterised Herbig Ae disks. The line-rich data we present motivates the need for more ALMA line surveys to probe the observable chemistry in Herbig Ae systems which offer unique insight into the composition of disk ices, including complex organic molecules.

### 5. An ALMA molecular inventory of warm Herbig Ae disks: II. Abundant complex organics and volatile sulphur in the IRS 48 disk

Alice S. Booth, Milou Temmink, Ewine F. van Dishoeck, Lucy Evans, John D. Ilee, Mihkel Kama, Luke Keyte, Charles J. Law, Margot Leemker, Nienke van der Marel, Hideko Nomura, Shota Notsu, Karin Öberg, Catherine Walsh ★ The Atacama Large Millimeter/submillimeter Array (ALMA) can probe the molecular content of planet-forming disks with unprecedented sensitivity. These observations allow us to build up an inventory of the volatiles available for forming planets and comets. Herbig Ae transition disks are fruitful targets due to the thermal sublimation of complex organic molecule (COM) and likely H<sub>2</sub>O-rich ices in these disks. The IRS 48 disk shows a

particularly rich chemistry that can be directly linked to its asymmetric dust trap. Here, we present ALMA observations of the IRS 48 disk where we detect 16 different molecules and make the first robust detections of H<sub>2</sub>13CO, 34SO, 33SO and c-H<sub>2</sub>COCH<sub>2</sub> (ethylene oxide) in a protoplanetary disk. All of the molecular emissions, aside from CO, are colocated with the dust trap and this includes newly detected simple molecules such as HCO<sup>+</sup>, HCN and CS. Interestingly, there are spatial offsets between different molecular families, including between the COMs and sulphur-bearing species, with the latter being more azimuthally extended and located radially further from the star. The abundances of the newly detected COMs relative to CH<sub>3</sub>OH are higher than the expected protostellar ratios, which implies some degree of chemical processing of the inherited ices during the disk lifetime. These data highlight IRS 48 as a unique astrochemical laboratory to unravel the full volatile reservoir at the epoch of planet and comet formation and the role of the disk in (re)setting chemical complexity.

## 6. JWST observations of <sup>13</sup>CO<sub>2</sub> ice: Tracing the chemical environment and thermal history of ices in protostellar envelopes

Nashanty G. C. Brunken, Will R. M. Rocha, Ewine F. van Dishoeck, Robert Gutermuth, Himanshu Tyagi, Katerina Slavicinska, Pooneh Nazari, S. Thomas Megeath, Neal J. Evans II, Mayank Narang, P. Manoj, Adam E. Rubinstein, Dan M. Watson, Leslie W. Looney, Harold Linnartz, Alessio Caratti o Garatti, Henrik Beuther, Hendrik Linz, Pamela Klaassen, Charles A. Poteet, Samuel Federman, Guillem Anglada, Prabhani Atnagulov, Tyler L. Bourke, William J. Fischer, Elise Furlan, Joel Green, Nolan Habel, Lee Hartmann, Nicole Karnath, Mayra Osorio, James Muzerolle Page, Riway Pokhrel, Rohan Rahatgaonkar, Patrick Sheehan, Thomas Stanke, Amelia M. Stutz, John J. Tobin, Lukasz Tychoniec, Scott Wolk, Yao-Lun Yang ★ The structure and composition of simple ices can be modified during stellar evolution by protostellar heating. Key to understanding the involved processes are thermal and chemical tracers that can diagnose the history and environment of the ice. The 15.2  $\mu$ m bending mode of <sup>12</sup>CO<sub>2</sub> has proven to be a valuable tracer of ice heating events but suffers from grain shape and size effects. A viable alternative tracer is the weaker <sup>13</sup>CO<sub>2</sub> isotopologue band at 4.39  $\mu$ m which has now become accessible at high S/N with the *James Webb* Space Telescope (JWST). We present JWST NIRSpec observations of <sup>13</sup>CO<sub>2</sub> ice in five deeply embedded Class 0 sources spanning a wide range in luminosities (0.2 - 10<sup>4</sup> L<sub>⊙</sub>) taken as part of the Investigating Protostellar Accretion Across the Mass Spectrum (IPA) program. The band profiles vary significantly, with the most luminous sources showing a distinct narrow peak at 4.38  $\mu$ m. We first apply a phenomenological approach and show that a minimum of 3-4 Gaussian profiles are needed to fit the <sup>13</sup>CO<sub>2</sub> absorption feature. We then combine these findings with laboratory data and show that a 15.2  $\mu$ m <sup>12</sup>CO<sub>2</sub> band inspired five-component decomposition can be applied for the isotopologue band where each component is representative of CO<sub>2</sub> ice in a specific molecular environment. The final solution consists of cold mixtures of CO<sub>2</sub> with CH<sub>3</sub>OH, H<sub>2</sub>O and CO as well as segregated heated pure CO<sub>2</sub> ice. Our results are in agreement with previous studies of the <sup>12</sup>CO<sub>2</sub> ice band, further confirming that <sup>13</sup>CO<sub>2</sub> is a useful alternative tracer of protostellar heating events. We also propose an alternative solution consisting only of heated CO<sub>2</sub>:CH<sub>3</sub>OH and CO<sub>2</sub>:H<sub>2</sub>O ices and warm pure CO<sub>2</sub> ice for decomposing the ice profiles of the two most luminous sources in our sample.

## 7. The dynamical evolution of star-forming regions measured with INDICATE

George A. Blaylock-Squibbs, Richard J. Parker ★ Observations of star-forming regions provide snapshots in time of the star formation process, and can be compared with simulation data to constrain the initial conditions of star formation. In order to make robust inferences, different metrics must be used to quantify the spatial and kinematic distributions of stars. In this paper, we assess the suitability of the INDICATE (INDEX to Define Inherent Clustering And Tendencies) method as a diagnostic to infer the initial conditions of star-forming regions that subsequently undergo dynamical evolution. We use INDICATE to measure the degree of clustering in N-body simulations of the evolution of star-forming regions with different initial conditions. We find that the clustering of individual stars, as measured by INDICATE, becomes significantly higher in simulations with higher initial stellar densities, and is higher in subvirial star-forming regions where significant amounts of dynamical mixing has occurred. We then combine INDICATE with other methods that measure the mass segregation, relative stellar surface density ratio and the morphology (Q-parameter) of star-forming regions, and show that the diagnostic capability of INDICATE increases when combined with these other metrics.

## 8. Deep Pa $\beta$ Imaging of the Candidate Accreting Protoplanet AB Aur b

Lauren I. Biddle, Brendan P. Bowler, Yifan Zhou, Kyle Franson, Zhoujian Zhang ★ Giant planets grow by accreting gas through circumplanetary disks, but little is known about the timescale and mechanisms involved in the planet assembly process because few accreting protoplanets have been discovered. Recent visible and infrared (IR) imaging revealed a potential accreting protoplanet within the transition disk around the young intermediate-mass Herbig Ae star, AB Aurigae (AB Aur). Additional imaging in H $\alpha$  probed for accretion and found agreement between the line-to-continuum flux ratio of the star and companion, raising the possibility that the emission source could be a compact disk feature seen in scattered starlight. We present new deep Keck/NIRC2 high-contrast imaging of AB Aur to characterize emission in Pa $\beta$ , another accretion tracer less subject to extinction. Our narrow band observations reach a  $5\sigma$  contrast of 9.6 mag at 0.6'', but we do not detect significant emission at the expected location of the companion, nor from other any other source in the system. Our upper limit on Pa $\beta$  emission suggests that if AB Aur b is a protoplanet, it is not heavily accreting or accretion is stochastic and was weak during the observations.

## 9. ALMA-IMF XI: The sample of hot core candidates A rich population of young high-mass proto-stars unveiled by the emission of methyl formate

M. Bonfand, T. Csengeri, S. Bontemps, N. Brouillet, F. Motte, F. Louvet, A. Ginsburg, N. Cunningham, R. Galván-Madrid, F. Herpin, F. Wyrowski, M. Vaille-Manet, A. M. Stutz, J. Di Francesco, A. Gusdorf, M. Fernández-López, B. Lefloch, H-L. Liu, P. Sanhueza, R. H. Álvarez-Gutiérrez, F. Olguin, T. Nony, A. Lopez-Sepulcre, P. Dell'Ova, Y. Pouteau, D. Jeff, H. -R. V. Chen, M. Armante, A. Towner, L. Bronfman, N. Kessler ★ Sites associated with high-mass star and cluster formation exhibit a so-called hot core phase, characterized by high temperatures and column densities of complex organic molecules. We built a comprehensive census of hot core candidates towards the ALMA-IMF protoclusters based on the detection of two CH<sub>3</sub>OCHO emission lines at 216.1 GHz. We used the source extraction algorithm GExt2D to identify peaks of methyl formate (CH<sub>3</sub>OCHO) emission that is a complex species commonly observed towards sites of star formation. We built up a catalog of 76 hot core candidates with masses ranging from about 0.2 to 80 Msun, of which 56 are new detections. A large majority of these objects are compact, rather circular, with deconvolved FWHM sizes of about 2300 au on average. About 30% of our sample of methyl formate sources have core masses above 8 Msun within sizes ranging from about 1000 au to 13400 au, which well correspond to archetypical hot cores. The origin of the CH<sub>3</sub>OCHO emission toward the lower-mass cores can be explained by a mixture of contribution from shocks, or may correspond to objects in a more evolved state, i.e. beyond the hot core stage. We find that the fraction of hot core candidates increases with the core mass. The large fraction of hot core candidates towards the most massive cores suggests that they rapidly enter the hot core phase and feedback effects from the forming protostar(s) impact their environment on short time-scales.

## 10. Protoplanet collisions: new scaling laws from SPH simulations

Samuele Crespi, Mohamad Ali-Dib, Ian Dobbs-Dixon ★ One common approach for solving collisions between protoplanets in simulations of planet formation is to employ analytical scaling laws. The most widely used one was developed by Leinhardt & Stewart (2012) from a catalog of 180 N-body simulations of rubble-pile collisions. In this work, we use a new catalogue of more than 20,000 SPH simulations to test the validity and the prediction capability of Leinhardt & Stewart (2012) scaling laws. We find that these laws overestimate the fragmentation efficiency in the merging regime and they are not able to properly reproduce the collision outcomes in the super-catastrophic regime. In the merging regime, we also notice a significant dependence between the collision outcome, in terms of the largest remnant mass, and the relative mass of the colliding protoplanets. Here, we present a new set of scaling laws that are able to better predict the collision outcome in all regimes and it is also able to reproduce the observed dependence on the mass ratio. We compare our new scaling laws against a machine learning approach and obtain similar prediction efficiency.

## 11. Thermal processing of primordial pebbles in evolving protoplanetary disks

Maria Jose Colmenares, Michiel Lambrechts, Elishevah van Kooten, Anders Johansen ★ During protoplanetary disk formation, dust grains located in the outer disk retain their pristine icy composition, while solids in the inner stellar-heated disk undergo volatile loss. This process may have left a fossil record in Solar System material showing different nucleosynthetic imprints that have been attributed to different degrees of thermal processing. However, it remains unclear how a large mass fraction of thermally-processed inner-disk pebbles is produced and how these grains

are subsequently transported throughout the disk. In this work we numerically investigate the evolution in time of a two-component pebble disk, consisting of pristine pebbles and those that underwent ice sublimation. We find that stellar outbursts exceeding 1000 times the solar luminosity are efficient in thermally altering, through ice sublimation, a large mass fraction of pebbles (around 80%). After the establishment of this initial radial dust composition gradient throughout the disk, the subsequent mixing and inward drift of pristine outer-disk pebbles alter the inner disk bulk composition from processed to more unprocessed in time. Therefore, if processed pebbles without ice mantles have an isotopic composition similar to ureilite meteorites from the inner Solar System, inner-disk minor bodies forming from the early pebble flux ( $<1\text{Myr}$ ) will be isotopically ureilite-like, while later-formed bodies will be increasingly admixed with the signature of the late incoming CI chondrite-like unprocessed pebbles. This appears to be largely consistent with the trend seen between the accretion age of different meteoric classes and their different stable isotope composition anomalies (in  $\mu^{54}\text{Cr}$ ,  $\mu^{48}\text{Ca}$ ,  $\mu^{30}\text{Si}$ ,  $\mu^{58}\text{Ni}$ ), but further work may be needed to explain the role of isotopically anomalous refractory inclusions and anomaly trends in other elements.

## 12. FAUST XII. Accretion streamers and jets in the VLA 1623–2417 protocluster

C. Codella, L. Podio, M. De Simone, C. Ceccarelli, S. Ohashi, C. J. Chandler, N. Sakai, J. E. Pineda, D. M. Segura-Cox, E. Bianchi, N. Cuello, A. López-Sepulcre, D. Fedele, P. Caselli, S. Charnley, D. Johnstone, Z. E. Zhang, M. J. Maureira, Y. Zhang, G. Sabatini, B. Svoboda, I. Jiménez-Serra, L. Loinard, S. Mercimek, N. Murillo, S. Yamamoto ★ The ALMA interferometer has played a key role in revealing a new component of the Sun-like star forming process: the molecular streamers, i.e. structures up to thousands of au long funneling material non-axisymmetrically to disks. In the context of the FAUST ALMA LP, the archetypical VLA1623-2417 protostellar cluster has been imaged at 1.3 mm in the SO( $5_6-4_5$ ), SO( $6_6-5_5$ ), and SiO( $5-4$ ) line emission at the spatial resolution of 50 au. We detect extended SO emission, peaking towards the A and B protostars. Emission blue-shifted down to  $6.6\text{ km s}^{-1}$  reveals for the first time a long ( $\sim 2000\text{ au}$ ) accelerating streamer plausibly feeding the VLA1623 B protostar. Using SO, we derive for the first time an estimate of the excitation temperature of an accreting streamer:  $33\pm 9\text{ K}$ . The SO column density is  $\sim 10^{14}\text{ cm}^{-2}$ , and the SO/H<sub>2</sub> abundance ratio is  $\sim 10^{-8}$ . The total mass of the streamer is  $3 \times 10^{-3}\text{ Msun}$ , while its accretion rate is  $3-5 \times 10^{-7}\text{ Msun yr}^{-1}$ . This is close to the mass accretion rate of VLA1623 B, in the  $0.6-3 \times 10^{-7}\text{ Msun yr}^{-1}$  range, showing the importance of the streamer in contributing to the mass of protostellar disks. The highest blue- and red-shifted SO velocities behave as the SiO( $5-4$ ) emission, the latter species detected for the first time in VLA1623-2417: the emission is compact (100-200 au), and associated only with the B protostar. The SO excitation temperature is  $\sim 100\text{ K}$ , supporting the occurrence of shocks associated with the jet, traced by SiO.

## 13. An Automated Chemical Exploration of NGC 6334I at 340 au Resolution

Samer J. El-Abd, Crystal L. Brogan, Todd R. Hunter, Kin Long Kelvin Lee, Ryan A. Loomis, Brett A. McGuire ★ Much of the information gleaned from observations of star-forming regions comes from the analysis of their molecular emission spectra, particularly in the radio regime. The time-consuming nature of fitting synthetic spectra to observations interactively for such line-rich sources, however, often results in such analysis being limited to data extracted from a single-dish observation or a handful of pixels from an interferometric observation. Yet, star-forming regions display a wide variety of physical conditions that are difficult, if not impossible, to accurately characterize with such a limited number of spectra. We have developed an automated fitting routine that visits every pixel in the field of view of an ALMA data cube and determines the best-fit physical parameters, including excitation temperature and column densities, for a given list of molecules. In this proof-of-concept work, we provide an overview of the fitting routine and apply it to  $0''.26$ ,  $1.1\text{ km s}^{-1}$  resolution ALMA observations of two sites of massive star-formation in NGC 6334I. Parameters were found for 21 distinct molecules by generating synthetic spectra across 7.48 GHz of spectral bandwidth between 280 and 351 GHz. Spatial images of the derived parameters for each of the  $> 8000$  pixels are presented with special attention paid to the C<sub>2</sub>H<sub>4</sub>O<sub>2</sub> isomers and their relative variations. We highlight the greater scientific utility of the column density and velocity images of individual molecules compared to traditional moment maps of single transitions.

#### 14. The 3D structure of disc-instability protoplanets

Adam Fenton, Dimitris Stamatellos ★ Context. The model of disc fragmentation due to gravitational instabilities offers an alternate formation mechanism for gas giant planets, especially those on wide orbits. Aims. Our goal is to determine the 3D structure of disc-instability protoplanets and to examine how this relates to the thermal physics of the fragmentation process. Methods. We modelled the fragmentation of gravitationally unstable discs using the SPH code PHANTOM, and followed the evolution of the protoplanets formed through the first and second-hydrostatic core phases (up to densities  $1\text{e-3 g/cm}^3$ ). Results. We find that the 3D structure of disc-instability protoplanets is affected by the disc environment and the formation history of each protoplanet (e.g. interactions with spiral arms, mergers). The large majority of the protoplanets that form in the simulations are oblate spheroids rather than spherical, and they accrete faster from their poles. Conclusions. The 3D structure of disc-instability protoplanets is expected to affect their observed properties and should be taken into account when interpreting observations of protoplanets embedded in their parent discs.

#### 15. Stellar companions and Jupiter-like planets in young associations

R. Gratton, M. Bonavita, D. Mesa, S. Desidera, A. Zurlo, S. Marino, V. D'Orazi, E. Rigliaco, V. Nascimbeni, D. Barbato, G. Columba, V. Squicciarini ★ Recently, combining high-contrast imaging and space astrometry we found that Jupiter-like (JL) planets are frequent in the beta Pic moving group (BPMG) around those stars where their orbit can be stable, prompting further analysis and discussion. We broaden our previous analysis to other young nearby associations to determine the frequency, mass, and separation of companions in general and JL in particular and their dependencies on the mass and age of the associations. We collected available data about companions including those revealed by visual observations, eclipses, spectroscopy, and astrometry. We determined search completeness and found that it is very high for stellar companions, while completeness corrections are still large for JL companions. Once these corrections are included, we found a high frequency of companions, both stellar ( $>0.52\pm0.03$ ) and JL ( $0.57\pm0.11$ ). The two populations are separated by a gap that corresponds to the brown dwarf desert. Within the population of massive companions, we found trends in frequency, separation, and mass ratios with stellar mass. Planetary companions pile up in the region just outside the ice line and we found them to be frequent once completeness was considered. The frequency of JL planets decreases with the overall mass and possibly the age of the association. We tentatively identify the two populations as due to disk fragmentation and core accretion, respectively. The distributions of stellar companions with a semi-major axis  $<1000$  au is well reproduced by a simple model of formation by disk fragmentation. The observed trends with stellar mass can be explained by a shorter but much more intense phase of accretion onto the disk of massive stars and by a more steady and prolonged accretion on solar-type stars. Possible explanations for the trends in the population of JL planets with association mass and age are briefly discussed.

#### 16. Search for Brown Dwarfs in IC 1396 with Subaru HSC: Interpreting the Impact of Environmental Factors on Sub-stellar Population

Saumya Gupta, Jessy Jose, Swagat Ranjan Das, Zhen Guo, Belinda Damian, Prem Prakash, Manash Ranjan Samal ★ Young stellar clusters are predominantly the hub of star formation and hence, ideal to perform comprehensive studies over the least explored sub-stellar regime. Various unanswered questions like the mass distribution in brown dwarf regime and the effect of diverse cluster environment on brown dwarf formation efficiency still plague the scientific community. The nearby young cluster, IC 1396 with its feedback-driven environment, is ideal to conduct such study. In this paper we adopt a multi-wavelength approach, using deep Subaru HSC, Gaia DR3, Pan-STARRS, UKIDSS/2MASS photometry and machine learning techniques to identify the cluster members complete down to  $\sim 0.03 M_{\odot}$  in the central  $22'$  area of IC 1396. We identify 458 cluster members including 62 brown dwarfs which are used to determine mass distribution in the region. We obtain a star-to-brown dwarf ratio of  $\sim 6$  for a stellar mass range  $0.03 - 1 M_{\odot}$  in the studied cluster. The brown dwarf fraction is observed to increase across the cluster as radial distance from the central OB-stars increases. This study also compiles 15 young stellar clusters to check the variation of star-to-brown dwarf ratio relative to stellar density and UV flux ranging within  $4\text{-}2500 \text{ stars pc}^{-2}$  and  $0.7\text{-}7.3 G_{\odot}$  respectively. The brown dwarf fraction is observed to increase with stellar density but the results about the influence of incident UV flux are inconclusive within this range. This is the deepest study of IC 1396 as of yet and it will pave the way to understand various aspects of brown dwarfs using spectroscopic observations in future.

17. **Implications of the discovery of AF Lep b: The mass-luminosity relation for planets in the  $\beta$  Pic Moving Group and the L-T transition for young companions and free-floating planets**

R. Gratton, M. Bonavita, D. Mesa, A. Zurlo, S. Marino, S. Desidera, V. D'Orazi, E. Rigliaco, V. Squicciarini, P. H. Nogueira ★ Dynamical masses of young planets aged between 10 and 200 Myr detected in imaging play a crucial role in shaping models of giant planet formation. Regrettably, only a few such objects possess these characteristics. Furthermore, the evolutionary pattern of young sub-stellar companions in near-infrared colour-magnitude diagrams might diverge from free-floating objects, possibly due to differing formation processes. The recent identification of a giant planet around AF Lep, part of the beta Pic moving group (BPMG), encouraged us to re-examine these points. We considered updated dynamical masses and luminosities for the sub-stellar objects in the BPMG. In addition, we compared the properties of sub-stellar companions and free-floating objects in the BPMG and other young associations remapping the positions of the objects in the colour-magnitude diagram into a dustiness-temperature plane. We found that cold-start evolutionary models do not reproduce the mass-luminosity relation for sub-stellar companions in the BPMG. This aligns rather closely with predictions from 'hot start' scenarios and is consistent with recent planet formation models. We obtain rather good agreement with masses from photometry and the remapping approach compared to actual dynamical masses. We also found a strong suggestion that the near-infrared colour-magnitude diagram for young companions is different from that of free-floating objects belonging to the same young associations. If confirmed by further data, this last result would imply that cloud settling - which likely causes the transition between L and T spectral type - occurs at a lower effective temperature in young companions than in free-floating objects. This might tentatively be explained with a different chemical composition.

18. **Constraining Planetary Formation Models Using Conditional Occurrences of Various Planet Types**

Sridhar Gajendran, Ing-Guey Jiang, Li-Chin Yeh, Devesh P. Saria ★ We report the conditional occurrences between three planetary types: super-Earths ( $m \sin i < 10 M_{\oplus}$ ,  $P < 100$  days), warm Jupiters ( $m \sin i > 95 M_{\oplus}$ ,  $10 < P < 100$  days), and cold Jupiters ( $m \sin i > 95 M_{\oplus}$ ,  $P > 400$  days) for sun-like stars. We find that while the occurrence of cold Jupiters in systems with super-Earths is  $22.2^{+8.3}_{-5.4}\%$ , compared to 10% for the absolute occurrence rate of cold Jupiters, the occurrence of super-Earths in systems with cold Jupiters is  $66.0^{+18.0}_{-16.0}\%$ , compared to 30% for the absolute occurrence rate of super-Earths for sun-like stars. We find that the enhancement of super-Earths in systems with cold Jupiters is evident for sun-like stars, in agreement with several previous studies. We also conduct occurrence studies between warm Jupiters and super-Earths, and between warm Jupiters and cold Jupiters, to consolidate our methods. We conduct an independent observational test to study the effects of cold Jupiters against the inner multiplicity using the well-established giant planet host star metallicity correlation for all transiting planets found to date. The conditional occurrences we find here can be used to constrain the validity of various planetary formation models. The extremely interesting correlations between the super-Earths, cold Jupiters, and warm Jupiters can also be used to understand the formation histories of these planetary types.

19. **Multi-wavelength detection of an ongoing FUOr-type outburst on a low-mass YSO**

Zhen Guo, P. W. Lucas, R. G. Kurtev, J. Borissova, V. Elbakyan, C. Morris, A. Bayo, L. Smith, A. Caratti o Garatti, C. Contreras Peña, D. Minniti, J. Jose, M. Ashraf, J. Alonso-García, N. Miller, H. D. S. Muthu ★ During the pre-main-sequence evolution, Young Stellar Objects (YSOs) assemble most of their mass during the episodic accretion process. The rarely seen FUOr-type events (FUOrs) are valuable laboratories to investigate the outbursting nature of YSOs. Here, we present multi-wavelength detection of a high-amplitude eruptive source in the young open cluster VdBH 221 with an ongoing outburst, including optical to mid-infrared time series and near-infrared spectra. The initial outburst has an exceptional amplitude of  $>6.3$  mag in Gaia and 4.6 mag in  $K_s$ , with a peak luminosity up to  $16 L_{\odot}$  and a peak mass accretion rate of  $1.4 \times 10^{-5} M_{\odot} \text{ yr}^{-1}$ . The optical to infrared spectral energy distribution (SED) of this object is consistent with a low-mass star ( $0.2 M_{\odot}$ ) with a modest extinction ( $A_V < 2$  mag). A 100-d delay between optical and infrared rising stages is detected, suggesting an outside-in origin of the instability. The spectroscopic features of this object reveal a self-luminous accretion disc, very similar to FU Orionis, with a low line-of-sight extinction. Most recently, there has been a gradual increase in brightness throughout the wavelength range, possibly suggesting an enhancement of the mass accretion rate.

**20. Spectroscopic confirmation of high-amplitude eruptive YSOs and dipping giants from the VVV survey**

Zhen Guo, P. W. Lucas, R. Kurtev, J. Borissova, C. Contreras Peña, S. N. Yurchenko, L. C. Smith, D. Minniti, R. K. Saito, A. Bayo, M. Catelan, J. Alonso-García, A. Caratti o Garatti, C. Morris, D. Froebrich, J. Tennyson, K. Maucó, A. Aguayo, N. Miller, H. D. S. Muthu ★ During the pre-main-sequence (pre-MS) evolution stage of a star, significant amounts of stellar mass are accreted during episodic accretion events, such as multi-decade FUor-type outbursts. Here, we present a near-infrared spectroscopic follow-up study of 33 high-amplitude (most with  $\Delta K_s > 4$  mag) variable sources discovered by the Vista Variables in the Via Lactea (VVV) survey. Based on the spectral features, 25 sources are classified as eruptive young stellar objects (YSOs), including 15 newly identified FUors, six with long-lasting but EXor-like bursts of magnetospheric accretion and four displaying outflow-dominated spectra. By examining the photometric behaviours of eruptive YSOs, we found most FUor-type outbursts have higher amplitudes ( $\Delta K_s$  and  $\Delta W2$ ), faster eruptive timescales and bluer infrared colours than the other outburst types. In addition, we identified seven post-main sequence variables apparently associated with deep dipping events and an eruptive star with deep AIO absorption bands resembling those seen in the V838 Mon stellar merger.

**21. Cloudlet Capture Model for the Accretion Streamer onto the disk of DG Tau**

Tomoyuki Hanawa, Antonio Garufi, Linda Podio, Claudio Codella, Dominique Segura-Cox ★ DG Tau is a nearby T Tauri star associated with a collimated jet, a circumstellar disk and a streamer a few hundred au long. The streamer connects to the disk at  $\sim 50$  au from DG Tau. At this location SO emission is observed, likely due to the release of sulphur from dust grains caused by the shock of the impact of the accretion streamer onto the disk. We investigate the possibility that the DG Tau streamer was produced via cloudlet capture on the basis of hydrodynamic simulations, considering a cloudlet initiating infall at 600 au from DG Tau with low angular momentum so that the centrifugal force is smaller than the gravitational force, even at 50 au. The elongation of the cloudlet into a streamer is caused by the tidal force when its initial velocity is much less than the free-fall velocity. The elongated cloudlet reaches the disk and forms a high density gas clump. Our hydrodynamic model reproduces the morphology and line-of-sight velocity of CS (5 – 4) emission from the Northern streamer observed with ALMA. We discuss the conditions for forming a streamer based on the simulations. We also show that the streamer should perturb the disk after impact for several thousands of years.

**22. On the magnetic field properties of protostellar envelopes in Orion**

Bo Huang, Josep M. Girart, Ian W. Stephens, Manuel Fernandez-Lopez, Hector G. Arce, John M. Carpenter, Paulo Cortes, Erin G. Cox, Rachel Friesen, Valentin J. M. Le Gouellec, Charles L. H. Hull, Nicole Karnath, Woojin Kwon, Zhi-Yun Li, Leslie W. Looney, Tom Megeath, Philip C. Myers, Nadia M. Murillo, Jaime E. Pineda, Sarah Sadavoy, Alvaro Sanchez-Monge, Patricio Sanhueza, John J. Tobin, Qizhou Zhang, James M. Jackson, Dominique Segura-Cox ★ We present 870  $\mu$ m polarimetric observations toward 61 protostars in the Orion molecular clouds, with 400 au (1") resolution using the Atacama Large Millimeter/submillimeter Array. We successfully detect dust polarization and outflow emission in 56 protostars, in 16 of them the polarization is likely produced by self-scattering. Self-scattering signatures are seen in several Class 0 sources, suggesting that grain growth appears to be significant in disks at earlier protostellar phases. For the rest of the protostars, the dust polarization traces the magnetic field, whose morphology can be approximately classified into three categories: standard-hourglass, rotated-hourglass (with its axis perpendicular to outflow), and spiral-like morphology. 40.0% (+3.0%) of the protostars exhibit a mean magnetic field direction approximately perpendicular to the outflow on several 100–1000 au scales. However, in the remaining sample, this relative orientation appears to be random, probably due to the complex set of morphologies observed. Furthermore, we classify the protostars into three types based on the C17O (3–2) velocity envelope's gradient: perpendicular to outflow, non-perpendicular to outflow, and unresolved gradient ( $< 1.0$  km/s/arcsec). In protostars with a velocity gradient perpendicular to outflow, the magnetic field lines are preferentially perpendicular to outflow, most of them exhibit a rotated hourglass morphology, suggesting that the magnetic field has been overwhelmed by gravity and angular momentum. Spiral-like magnetic fields are associated with envelopes having large velocity gradients, indicating that the rotation motions are strong enough to twist the field lines. All of the protostars with a standard-hourglass field morphology show no significant velocity gradient due to the strong magnetic braking.

### 23. Chondrule Formation During Low-Speed Collisions of Planetesimals: A Hybrid Splash-Flyby Framework

William Herbst, James P. Greenwood ★ Chondrules probably formed during a small window of time  $\sim 1\text{--}4$  Ma after CAIs, when most solid matter in the asteroid belt was already in the form of km-sized planetesimals. They are unlikely, therefore, to be “building blocks” of planets or abundant on asteroids, but more likely to be a product of energetic events common in the asteroid belt at that epoch. Laboratory experiments indicate that they could have formed when solids of primitive composition were heated to temperatures of  $\sim 1600$  K and then cooled for minutes to hours. A plausible heat source for this is magma, which is likely to have been abundant in the asteroid belt at that time, and only that time, due to the trapping of  $^{26}\text{Al}$  decay energy in planetesimal interiors. Here we propose that chondrules formed during low-speed ( $\lesssim 1\text{ km s}^{-1}$ ) collisions between large planetesimals when heat from their interiors was released into a stream of primitive debris from their surfaces. Heating would have been essentially instantaneous and cooling would have been on the dynamical time scale,  $1/\sqrt{G\rho} \sim 30$  minutes, where  $\rho$  is the mean density of a planetesimal. Many of the heated fragments would have remained gravitationally bound to the merged object and could have suffered additional heating events as they orbited and ultimately accreted to its surface. This is a hybrid of the splash and flyby models: we propose that it was the energy released from a body’s molten interior, not its mass, that was responsible for chondrule formation by heating primitive debris that emerged from the collision.

### 24. An Episode of Occultation Events in Gaia21bcv

Klaus W. Hodapp, Eric Gaidos, Matthew A. Kenworthy, Michael Tucker, Benjamin J. Shappee, Anna V. Payne, Aaron Do ★ A previously unremarkable star near the Canis Major OB1/R1 association underwent an episode of multiple deep brightness minima. Light curves based on archival Gaia, ZTF, NEOWISE data and additional observations from LCO and UKIRT show that the star was not variable prior to 2019 Aug 18 (MJD 58700), and on that date started showing brightness dips of up to 3 magnitudes in the Gaia G and ZTF r bandpasses. After MJD 59500, 800 days after the onset of these dipping events, the star returned to its previous brightness, and no significant dipping events have been recorded since. Compared to the stable phase, NEOWISE infrared photometry in the W1 and W2 bands indicates a generally redder color, and both decreases and increases in brightness at different times during the dipping episode. The spectrum of Gaia21bcv taken after the end of the dipping episode shows several neutral and ionized metal absorption lines, including Li, indicating a spectral type of K5. Variable emission from [OI] was observed. The H alpha absorption in Gaia21bcv is too faint and irregular for this spectral type, indicating that the line is partly filled in by variable emission, a signature of weak episodic accretion. Gaia21bcv lies above the zero-age main sequence, but is much fainter than typical R CrB stars. We interpret the light curve of Gaia21bcv as being similar to the occultation events in Epsilon Aurigae, i.e., occultation by a disk around a companion object orbiting the primary star.

### 25. The outflow of the protostar in B335: I

Klaus W. Hodapp, Laurie L. Chu, Thomas Greene, Michael R. Meyer, Doug Johnstone, Marcia J. Rieke, John Stansberry, Martha Boyer, Charles Beichman, Scott Horner, Tom Roellig, George Rieke, Eric T. Young ★ The isolated globule B335 contains a single, low luminosity Class 0 protostar associated with a bipolar nebula and outflow system seen nearly perpendicular to its axis. We observed the innermost regions of this outflow as part of JWST/NIRCam GTO program 1187, primarily intended for wide-field slitless spectroscopy of background stars behind the globule. We find a system of expanding shock fronts with kinematic ages of only a few decades emerging symmetrically from the position of the embedded protostar, which is not directly detected at NIRCam wavelengths. The innermost and youngest of the shock fronts studied here shows strong emission from CO. The next older shock front shows less CO and the third shock front shows only H2 emission in our data. This third and most distant of these inner shock fronts shows substantial evolution of its shape since it was last observed with high spatial resolution in 1996 with Keck/NIRC. This may be evidence of a faster internal shock catching up with a slower one and of the two shocks merging.

## 26. Cloud-cloud collision and cluster formation in the W5-NW complex

Namitha Issac, Anindya Saha, Saanika Choudhary, Aakash Chaudhary, Anandmayee Tej, Hong-Li Liu, Tie Liu, Maheswar Gopinathan ★ We present a detailed structural and gas kinematic study of the star-forming complex W5-NW. A cloud-cloud collision scenario unravels with evidences of collision induced star and cluster formation. Various signatures of cloud-cloud collision such as "complementary distribution" and "bridging-features" are explored. At the colliding region, the two clouds have complementary morphologies, where W5-NWb has a filamentary key-like shape which fits into the U-shaped cavity in W5-NWa that behaves like a keyhole. The interaction region between the two clouds is characterised by bridging features with intermediate velocities connecting the two clouds. A skewed V-shaped bridging feature is also detected at the site of collision. A robust picture of the molecular gas distribution highlighting the bridges is seen in the position-position-velocity diagram obtained using the SCOUSEPY algorithm. Star cluster formation with an over-density of Class I and Class II young stellar objects is also seen towards this cloud complex, likely triggered by the cloud collision event.

## 27. Atmospheric Retrievals of the Young Giant Planet ROXs 42B b from Low- and High-Resolution Spectroscopy

Julie Inglis, Nicole L. Wallack, Jerry W. Xuan, Heather A. Knutson, Yayaati Chachan, Marta L. Bryan, Brendan P. Bowler, Aishwarya Iyer, Tiffany Kataria, Björn Benneke ★ Previous attempts have been made to characterize the atmospheres of directly imaged planets at low-resolution ( $R \sim 10\text{s}-100\text{s}$ ), but the presence of clouds has often led to degeneracies in the retrieved atmospheric abundances with cloud opacity and temperature structure that bias retrieved compositions. In this study, we perform retrievals on the ultra-young ( $\lesssim 5$  Myr) directly imaged planet ROXs 42B b with both a downsampled low-resolution *JHK*-band spectrum from Gemini/NIFS and Keck/OSIRIS, and a high-resolution *K*-band spectrum from pre-upgrade Keck/NIRSPAO. Using the atmospheric retrieval framework of petitRADTRANS, we analyze both data sets individually and combined. We additionally fit for the stellar abundances and other physical properties of the host stars, a young M spectral type binary, using the SPHINX model grid. We find that the measured C/O,  $0.50 \pm 0.05$ , and metallicity,  $[\text{Fe}/\text{H}] = -0.67 \pm 0.35$ , for ROXs 42B b from our high-resolution spectrum agree with that of its host stars within  $1\sigma$ . The retrieved parameters from the high-resolution spectrum are also independent of our choice of cloud model. In contrast, the retrieved parameters from the low-resolution spectrum show strong degeneracies between the clouds and the retrieved metallicity and temperature structure. When we retrieve on both data sets together, we find that these degeneracies are reduced but not eliminated, and the final results remain highly sensitive to cloud modeling choices. We conclude that high-resolution spectroscopy offers the most promising path for reliably determining atmospheric compositions of directly imaged companions independent of their cloud properties.

## 28. The Gaia-ESO Survey: Empirical estimates of stellar ages from lithium equivalent widths (EAGLES)

R. D. Jeffries, R. J. Jackson, Nicholas J. Wright, G. Weaver, G. Gilmore, S. Randich, A. Bragaglia, A. J. Korn, R. Smiljanic, K. Biazzo, A. R. Casey, A. Frasca, A. Gonneau, G. Guiglion, L. Morbidelli, L. Prisinzano, G. G. Sacco, G. Tautvaišienė, C. C. Worley, S. Zaggia ★ We present an empirical model of age-dependent photospheric lithium depletion, calibrated using a large, homogeneously-analysed sample of 6200 stars in 52 open clusters, with ages from 2–6000 Myr and  $-0.3 < [\text{Fe}/\text{H}] < 0.2$ , observed in the Gaia-ESO spectroscopic survey. The model is used to obtain age estimates and posterior age probability distributions from measurements of the Li I 6708Å equivalent width for individual (pre) main sequence stars with  $3000 < T_{\text{eff}}/\text{K} < 6500$ , a domain where age determination from the HR diagram is either insensitive or highly model-dependent. In the best cases, precisions of 0.1 dex in log age are achievable; even higher precision can be obtained for coeval groups and associations where the individual age probabilities of their members can be combined. The method is validated on a sample of exoplanet-hosting young stars, finding agreement with claimed young ages for some, but not others. We obtain better than 10 per cent precision in age, and excellent agreement with published ages, for seven well-studied young moving groups. The derived ages for young clusters ( $< 1$  Gyr) in our sample are also in good agreement with their training ages, and consistent with several published, model-insensitive lithium depletion boundary ages. For older clusters there remain systematic age errors that could be as large as a factor of two. There is no evidence to link these errors to any strong systematic metallicity dependence of (pre) main sequence lithium depletion, at least in the range  $-0.29 < [\text{Fe}/\text{H}] < 0.18$ . Our methods and model are provided as software – "Empirical AGes from Lithium Equivalent widthS" (EAGLES).

## 29. The Radcliffe Wave is Oscillating

Ralf Konietzka, Alyssa A. Goodman, Catherine Zucker, Andreas Burkert, João Alves, Michael Foley, Cameren Swiggum, Maria Koller, Núria Miret-Roig ★ Our Sun lies within 300 pc of the 2.7-kpc-long sinusoidal chain of dense gas clouds known as the Radcliffe Wave. The structure’s wave-like shape was discovered using 3D dust mapping, but initial kinematic searches for oscillatory motion were inconclusive. Here we present evidence that the Radcliffe Wave is oscillating through the Galactic plane while also drifting radially away from the Galactic Center. We use measurements of line-of-sight velocity for 12CO and 3D velocities of young stellar clusters to show that the most massive star-forming regions spatially associated with the Radcliffe Wave (including Orion, Cepheus, North America, and Cygnus X) move as if they are part of an oscillating wave driven by the gravitational acceleration of the Galactic potential. By treating the Radcliffe Wave as a coherently oscillating structure, we can derive its motion independently of the local Galactic mass distribution, and directly measure local properties of the Galactic potential as well as the Sun’s vertical oscillation period. In addition, the measured drift of the Radcliffe Wave radially outward from the Galactic Center suggests that the cluster whose supernovae ultimately created today’s expanding Local Bubble may have been born in the Radcliffe Wave.

## 30. Magnetic fields of protoplanetary disks

Sergey A. Khaibrakhmanov ★ We review the current status of studies on accretion and protoplanetary disks of young stars with large-scale magnetic fields. Observational data on magnetic fields of the disks are compiled and analysed. Modern analytical and numerical MHD models of protoplanetary disks are discussed. The mechanisms of angular momentum transport via turbulence, magnetic tensions and outflows are outlined. We consider the influence of Ohmic dissipation, magnetic ambipolar diffusion, magnetic buoyancy, and the Hall effect on the evolution of the magnetic flux in disks. Modern MHD models of accretion disks show that the magnetic field can influence the structure of protoplanetary disks. We argue that the available observational data on the magnetic fields in protoplanetary disks can be interpreted within the framework of fossil magnetic field theory. We summarize the problems of the modern theory of accretion and protoplanetary disks with magnetic fields and also outline the prospects for further research.

## 31. SMA detection of an extreme millimeter flare from the young class III star HD 283572

Joshua Bennett Lovell, Garrett K. Keating, David J. Wilner, Sean M. Andrews, Meredith MacGregor, Ramisa Akther Rahman, Ramprasad Rao, Jonathan P. Williams ★ We present evidence of variable 1.3 millimeter emission from the 1-3 Myr, SpT G2-G5 class III YSO, HD 283572. HD 283572 was observed on 8 dates with the Submillimeter Array between 2021 December and 2023 May, a total on-source time of 10.2 hours, probing a range of timescales down to 5.2 seconds. Averaging all data obtained on 2022 Jan 17 shows a 4.4 mJy ( $8.8\sigma$ ) point source detection with a negative spectral index ( $\alpha = -2.7 \pm 1.2$ ), with peak emission rising to 13.8 mJy in one 3 minute span, and 25 mJy in one 29.7 second integration ( $L_\nu = 4.7 \times 10^{17} \text{ erg s}^{-1} \text{ Hz}^{-1}$ ). Combining our data for the other 7 dates shows no detection, with an rms noise of 0.24 mJy beam $^{-1}$ . The stochastic millimeter enhancements on time frames of seconds–minutes–hours with negative spectral indices are most plausibly explained by synchrotron or gyro-synchrotron radiation from stellar activity. HD 283572’s 1.3 mm light-curve has similarities with variable binaries, suggesting HD 283572’s activity may have been triggered by interactions with an as-yet undetected companion. We additionally identify variability of HD 283572 at 10 cm, from VLASS data. This study highlights the challenges of interpreting faint mm emission from evolved YSOs that may host tenuous disks, and suggests that a more detailed temporal analysis of spatially unresolved data is generally warranted. The variability of class III stars may open up new ground for understanding the physics of flares in the context of terrestrial planet formation.

## 32. Forming localized dust concentrations in a dust ring: DM Tau case study

Hauyu Baobab Liu, Takayuki Muto, Mihoko Konishi, Chia-Ying Chung, Jun Hashimoto, Kiyooki Doi, Ruobing Dong, Tomoyuki Kudo, Yasuhiro Hasegawa, Yuka Terada, Akimasa Kataoka ★ The previous, high angular resolution 225 GHz ( $\sim 1.3$  mm) continuum observations on the transitional disk DM Tau have resolved an outer ring at 20-120 au radii that is weakly azimuthally asymmetric. We aimed to examine dust growth and filtration in the outer ring. We performed the  $\sim 0''.06$  ( $\sim 8.7$  au) resolution Karl G. Jansky Very Large Array (JVLA) 40-48 GHz ( $\sim 7$  mm; Q band) continuum observations and the complementary observations at lower frequencies. In addition, we analyzed the archival JVLA observations that were taken since 2010. Intriguingly, the Q band image resolved the azimuthally highly asymmetric, knotty dust emission sources close to the inner edge of the outer ring. Fitting the

8-700 GHz spectral energy distribution (SED) with two dust components indicates that the maximum grain size in these knotty dust emission sources is likely  $\gtrsim 300 \mu\text{m}$  while it is  $\lesssim 50 \mu\text{m}$  in the rest of the ring. These results may be explained by trapping of inward migrating grown dust close to the ring inner edge. The exact mechanism for developing the azimuthal asymmetry has not yet been identified, which may be due to planet-disk interaction that might also be responsible for the creation of the dust cavity and pressure bump, or the fluid instabilities and vortex formation due to shear motions. Finally, we remark that the asymmetries in DM Tau are hard to diagnose from the  $\gtrsim 225$  GHz observations owing to a high optical depth at the ring. In other words, the apparent symmetric or asymmetric morphology of the transitional disks may be related to the optical depths of those disks at the observing frequency.

### 33. **Spatial Variations of Dust Opacity and Grain Growth in Dark Clouds: L1689, L1709 and L1712**

Jun Li, Biwei Jiang, He Zhao, Xi Chen, Yang Yang ★ The far-infrared (FIR) opacity of dust in dark clouds within the Ophiuchus molecular cloud is investigated through multi-wavelength infrared observations from UKIDSS, Spitzer and Herschel. Employing the infrared color excess technique with both near-infrared (NIR) and mid-infrared (MIR) photometric data, a high-resolution extinction map in the  $K$  band ( $A_K$ ) is constructed for three dark clouds: L1689, L1709, and L1712. The derived extinction map has a resolution of  $1'$  and reaches a depth of  $A_K \sim 3$  mag. The FIR optical depths  $\tau_{250}$  at a reference wavelength of  $250 \mu\text{m}$  are obtained by fitting the Herschel PACS and SPIRE continuum data at 100, 160, 250, 350 and  $500 \mu\text{m}$  using a modified blackbody model. The average dust opacity per unit gas mass at  $250 \mu\text{m}$ ,  $\kappa_{250}$  is determined through a pixel-by-pixel correlation of  $\tau_{250}$  with  $A_K$ , yielding a value of approximately  $0.09 \text{ cm}^2 \text{ g}^{-1}$ , which is about 2-3 times higher than the typical value in the diffuse interstellar medium (ISM). Additionally, an independent analysis across 16 sub-regions within the Ophiuchus cloud indicates spatial variations in dust opacity, with values ranging from  $0.07$ - $0.12 \text{ cm}^2 \text{ g}^{-1}$ . Although the observed trend of increasing dust opacity with higher extinction implies grain growth, our findings indicate that rapid grain growth clearly not yet occurred in the dark clouds studied in this work.

### 34. **Dust Accumulation near the Magnetospheric Truncation of Protoplanetary Discs. II. The Effects of Opacity and Thermal Evolution**

Rixin Li, Yi-Xian Chen, Douglas N. C. Lin ★ Dust trapping in the global pressure bump induced by magnetospheric truncation offers a promising formation mechanism for close-in super-Earths/sub-Neptunes. These planets likely form in evolved protoplanetary discs, where the gas temperature at the expanding truncation radius become amiable to refractory solids. However, dust accumulation may alter the disc opacity such that thermal evolution is inevitable. To better understand how thermodynamics affects this planet formation pathway, we conduct a suite of local dust evolution simulations in an idealized inner disc model. Our calculations take into account self-consistent opacity-dependent temperature changes as well as dust evaporation and vapour condensation. We find that disc thermal evolution regulates dust growth and evolution, discouraging any accumulation of small particles that drives the increase of opacity and temperature. Significant retention of dust mass takes place when the disc environments allow runaway growth of large solids beyond the fragmentation barrier, where small particles are then swept up and preserved. Our results further validate dust accumulation near disc truncation as a promising mechanism to form close-in planets.

### 35. **Observations of high-order multiplicity in a high-mass stellar protocluster**

Shanghuo Li, Patricio Sanhueza, Henrik Beuther, Huei-Ru Vivien Chen, Rolf Kuiper, Fernando A. Olguin, Ralph E. Pudritz, Ian W. Stephens, Qizhou Zhang, Fumitaka Nakamura, Xing Lu, Rajika L. Kuruwita, Takeshi Sakai, Thomas Henning, Kotomi Taniguchi, Fei Li ★ The dominant mechanism forming multiple stellar systems in the high-mass regime ( $M_* \gtrsim 8 M_\odot$ ) remained unknown because direct imaging of multiple protostellar systems at early phases of high-mass star formation is very challenging. High-mass stars are expected to form in clustered environments containing binaries and higher-order multiplicity systems. So far only a few high-mass protobinary systems, and no definitive higher-order multiples, have been detected. Here we report the discovery of one quintuple, one quadruple, one triple and four binary protostellar systems simultaneously forming in a single high-mass protocluster, G333.23-0.06, using Atacama Large Millimeter/submillimeter Array high-resolution observations. We present a new example of a group of gravitationally bound binary and higher-order multiples during their early formation phases in a protocluster. This provides the clearest direct measurement of the initial configuration of primordial high-order multiple systems,

with implications for the in situ multiplicity and its origin. We find that the binary and higher-order multiple systems, and their parent cores, show no obvious sign of disk-like kinematic structure. We conclude that the observed fragmentation into binary and higher-order multiple systems can be explained by core fragmentation, indicating its crucial role in establishing the multiplicity during high-mass star cluster formation.

### 36. **JWST-MIRI Spectroscopy of Warm Molecular Emission and Variability in the AS 209 Disk**

Carlos E. Muñoz-Romero, Karin I. Öberg, Andrea Banzatti, Klaus M. Pontoppidan, Sean M. Andrews, David J. Wilner, Edwin A. Bergin, Ian Czekala, Charles J. Law, Colette Salyk, Richard Teague, Chunhua Qi, Jennifer B. Bergner, Jane Huang, Catherine Walsh, Viviana V. Guzmán, L. Ilse-dore Cleaves, Yuri Aikawa, Jaehan Bae, Alice S. Booth, Gianni Cataldi, John D. Ilee, Romane Le Gal, Feng Long, Ryan A. Loomis, François Menard, Yao Liu ★ We present MIRI MRS observations of the large, multi-gapped protoplanetary disk around the T-Tauri star AS 209. The observations reveal hundreds of water vapor lines from 4.9 to 25.5  $\mu\text{m}$  towards the inner  $\sim 1$  au in the disk, including the first detection of ro-vibrational water emission in this disk. The spectrum is dominated by hot ( $\sim 800$  K) water vapor and OH gas, with only marginal detections of CO<sub>2</sub>, HCN, and a possible colder water vapor component. Using slab models with a detailed treatment of opacities and line overlap, we retrieve the column density, emitting area, and excitation temperature of water vapor and OH, and provide upper limits for the observable mass of other molecules. Compared to MIRI spectra of other T-Tauri disks, the inner disk of AS 209 does not appear to be atypically depleted in CO<sub>2</sub> nor HCN. Based on *Spitzer IRS* observations, we further find evidence for molecular emission variability over a 10-year baseline. Water, OH, and CO<sub>2</sub> line luminosities have decreased by factors 2-4 in the new MIRI epoch, yet there are minimal continuum emission variations. The origin of this variability is yet to be understood.

### 37. **High-resolution ALMA observations of compact discs in the wide-binary system Sz 65 and Sz 66**

J. M. Miley, J. Carpenter, R. Booth, J. Jennings, T. J. Haworth, M. Vioque, S. Andrews, D. Wilner, M. Benisty, J. Huang, L. Perez, V. Guzman, L. Ricci, A. Isella ★ Substructures in disc density are ubiquitous in the bright extended discs that are observed with high resolution. These substructures are intimately linked to the physical mechanisms driving planet formation and disc evolution. Surveys of star-forming regions find that most discs are in fact compact, less luminous, and do not exhibit these same substructures. It remains unclear whether compact discs also have similar substructures or if they are featureless. This suggests that different planet formation and disc evolution mechanisms operate in these discs. We investigated evidence of substructure within two compact discs around the stars Sz 65 and Sz 66 using high angular resolution observations with ALMA at 1.3 mm. The two stars form a wide-binary system with 6.36 arcsec separation. The continuum observations achieve a synthesised beam major axis of 0.026 arcsec, equivalent to about 4.0 au, enabling a search for substructure on these spatial scales and a characterisation of the gas and dust disc sizes with high precision. We analysed the data in the image plane through an analysis of reconstructed images, as well as in the uv plane by modelling the visibilities and by an analysis of the 12CO emission line. Comparisons were made with high-resolution observations of compact discs and radially extended discs. We find evidence of substructure in the dust distribution of Sz 65, namely a shallow gap centred at approximately 20 au, with an emission ring exterior to it. Ninety percent of the measured continuum flux is found within 27 au, and the distance for 12CO is 142 au. The observations show that Sz 66 is very compact: 90 per cent of the continuum flux is contained within 16 au, and 48 au for the gas. While the overall prevalence and diversity of substructure in compact discs relative to larger discs is yet to be determined, we find evidence that substructures can exist in compact discs.

### 38. **Angular Momentum Transport in Binary Star Formation: The Enhancement of Magneto-Rotational Instability and Role of Outflows**

Tomoaki Matsumoto ★ The formation of binary stars is highly influenced by magnetic fields, which play a crucial role in transporting angular momentum. We conducted three-dimensional numerical simulations of binary star accretion via a circumbinary disk, taking into account a magnetic field perpendicular to the disk and an infalling envelope. Our simulations reproduce the following phenomena: (1) spiral arms associated with circumstellar disks, (2) turbulence in the circumbinary disk, induced by magneto-rotational instability (MRI), (3) a fast outflow launched from each circumstellar disk, and (4) a slow outflow from the circumbinary disk. The binary models exhibit a higher  $\alpha$ -parameter

than the corresponding single star models, indicating that the binary stars enhance MRI turbulence. Moreover, an infalling envelope also enhance the turbulence, leading to a high  $\alpha$ -parameter. While the spiral arms promotes radial flow, causing transfer of mass and angular momentum within the circumbinary disk, the MRI turbulence and outflows are main drivers of angular momentum transfer to reduce the specific angular momentum of the system.

### 39. Rotation curves in protoplanetary disks with thermal stratification

Paola Martire, Cristiano Longarini, Giuseppe Lodato, Giovanni P. Rosotti, Andrew Winter, Stefano Facchini, Caitlyn Hardiman, Myriam Benisty, Jochen Stadler, Andrés F. Izquierdo, Leonardo Testi ★ In recent years the gas kinematics probed by molecular lines detected with ALMA has opened a new window to study protoplanetary disks. High spatial and spectral resolution observations have revealed the complexity of protoplanetary disk structure and correctly interpreting these data allow us to gain a better comprehension of the planet formation process. We investigate the impact of thermal stratification on the azimuthal velocity of protoplanetary disks. High resolution gas observations are showing velocity differences between CO isotopologues, which cannot be adequately explained with vertically isothermal models. The aim of this work is to determine whether a stratified model can explain this discrepancy. We analytically solve the hydrostatic equilibrium for a stratified disk and we derive the azimuthal velocity. We test the model with SPH numerical simulations and then we use it to fit for star mass, disk mass and scale radius of the sources in the MAPS sample. In particular, we use  $^{12}\text{CO}$  and  $^{13}\text{CO}$  datacubes.

### 40. Aeolian erosion in protoplanetary discs: How impactful it is on dust evolution?

Stéphane Michoulier, Jean-François Gonzalez, Evgeni Grishin, Clément Petetin ★ Context: Many barriers prevent dust to form planetesimals via coagulation in protoplanetary discs, such as bouncing, collisional fragmentation or aeolian erosion. Modelling dust and the different phenomena that can alter its evolution is therefore needed. Multiple solutions have been proposed, but still need to be confirmed. Aims: In this paper, we explore the role aeolian erosion plays in the evolution of dust. Methods: We use a monodisperse model to account for dust growth and fragmentation, implemented in a 1D model to compute the evolution of single grains and a 3D SPH code to compute the global evolution of dust and gas. We test the erosion model in our code and ensured it matches previous results. Results: With a model of disc reproducing observations, we show with both 1D and 3D studies that erosion is not significant during the evolution of dust when we take fragmentation into consideration. With a low-viscosity disc, fragmentation is less of a problem, but grain growth is also less important, preventing the formation of large objects anyway. In dust traps, close to the star, erosion is also not impactful, even when fragmentation is turned off. Conclusions: We show in this paper that aeolian erosion is negligible when radial drift, fragmentation and dust traps are taken into account and does not alter the dust evolution in the disc. However, it can have an impact on later stages, i.e. when the streaming instability forms large clumps close to the star, or when planetesimals are captured.

### 41. New method for estimating molecular cloud distances based on Gaia, 2MASS, and the TRILEGAL galaxy model

Juan Mei, Zhiwei Chen, Zhibo Jiang, Sheng Zheng, Haoran Feng ★ We propose a new method for estimating the distances of molecular clouds traced by CO line emission. Stars from 2MASS and Gaia EDR3 are selected as on-cloud stars when they are projected on a cloud. The background on-cloud stars have redder colors on average than the foreground stars. Instead of searching for stars projected away from the cloud, we employed the TRILEGA galaxy model to mimic the stellar population without cloud extinction along the sightline toward the cloud. Our method does not require an exact boundary of a cloud. The boundaries are highly variable and depend on the sensitivity of the molecular line data. For each cloud, we compared the distributions of on-cloud stars to the TRILEGAL stellar populations in the diagram of  $J - K_s$  color versus distance. The intrinsic  $J - K_s$  colors of main-sequence and evolved stars from TRILEGAL were considered separately, and they were used as the baseline for subtracting the observed  $J - K_s$  colors. The baseline-corrected  $J - K_s$  color was deployed with the Bayesian analysis and Markov chain Monte Carlo sampling to determine the distance at which the  $J - K_s$  color jump is largest. This method was successfully applied to measure the distances of 27 molecular clouds, which were selected from previously published cloud samples. By replacing TRILEGAL with the GALAXIA galaxy model, we were able to measure the distances for 21 of the 27 clouds. The distances of the 21 clouds based on the GALAXIA model agree well with those based on the TRILEGAL model. The distances of the 27 clouds estimated by this method are consistent with previous estimates. We will apply this new method to a larger region of the gaseous galactic plane, in particular, for the inner galactic region, where a

region free of CO emission is hard to separate from the crowded field of clouds.

#### 42. **ALMA view of the L1448-mm protostellar system on disk scales: CH<sub>3</sub>OH and H<sup>13</sup>CN as new disk wind tracers**

P. Nazari, B. Tabone, A. Ahmadi, S. Cabrit, E. F. van Dishoeck, C. Codella, J. Ferreira, L. Podio, Ł. Tychoniec, M. L. van Gelder ★ Protostellar disks are known to accrete, however, the exact mechanism that extracts the angular momentum and drives accretion in the low-ionization "dead" region of the disk is under debate. In recent years, magneto-hydrodynamic (MHD) disk winds have become a popular solution. Yet, observations of these winds require both high spatial resolution ( $\sim 10$  au) and high sensitivity, which has resulted in only a handful of MHD disk wind candidates so far. In this work we present high angular resolution ( $\sim 30$  au) ALMA observations of the emblematic L1448-mm protostellar system and find suggestive evidence for an MHD disk wind. The disk seen in dust continuum ( $\sim 0.9$  mm) has a radius of  $\sim 23$  au. Rotating infall signatures in H<sup>13</sup>CO<sup>+</sup> indicate a central mass of  $0.4 \pm 0.1 M_{\odot}$  and a centrifugal radius similar to the dust disk radius. Above the disk, we unveil rotation signatures in the outflow traced by H<sup>13</sup>CN, CH<sub>3</sub>OH, and SO lines and find a kinematical structure consistent with theoretical predictions for MHD disk winds. This is the first detection of an MHD disk wind candidate in H<sup>13</sup>CN and CH<sub>3</sub>OH. The wind launching region estimated from cold MHD wind theory extends out to the disk edge. The magnetic lever arm parameter would be  $\lambda_{\phi} \simeq 1.7$ , in line with recent non-ideal MHD disk models. The estimated mass-loss rate is  $\sim 4$  times the protostellar accretion rate ( $\dot{M}_{\text{acc}} \simeq 2 \times 10^{-6} M_{\odot}/\text{yr}$ ) and suggests that the rotating wind could carry enough angular momentum to drive disk accretion.

#### 43. **Gas Phase Ions in Protoplanetary Disks from Collisions of Solids**

Jakob Penner, Gerhard Wurm, Jens Teiser ★ Ionization is important for magnetohydrodynamics and chemistry in protoplanetary disks but known ionization sources are often weak along the midplane. We present, for the first time, data from a laboratory experiment, where we measure ions from colliding mm-basalt grains emitted into the surrounding gas phase. This positive detection implies that very basic collisions in early phases of planet formation are sources of ionization. The midplane of protoplanetary disks might be ionized despite the lack of intense radiation sources.

#### 44. **Accretion and magnetism on young eccentric binaries: DQ Tau and AK Sco**

Kim Pouilly, Axel Hahlin, Oleg Kochukhov, Julien Morin, Ágnes Kóspál ★ The accretion and ejection of mass in pre-main sequence (PMS) stars are key processes in stellar evolution as they shape the stellar angular momentum transport necessary for the stars' stability. Magnetospheric accretion onto classical T Tauri stars and low-mass PMS stars has been widely studied in the single-star case. This process can not be directly transferred to PMS binary systems, as tidal and gravitation effects, and/or accretion from a circumbinary disc (with variable separation of the components in the case of eccentric orbits) are in place. This work examines the accretion process of two PMS eccentric binaries, DQ Tau and AK Sco, using high-resolution spectropolarimetric time series. We investigate how magnetospheric accretion can be applied to these systems by studying the accretion-related emission lines and the magnetic field of each system. We discover that both systems are showing signs of magnetospheric accretion, despite their slightly different configurations, and the weak magnetic field of AK Sco. Furthermore, the magnetic topology of DQ Tau A shows a change relative to the previous orbital cycle studied: previously dominated by the poloidal component, it is now dominated by the toroidal component. We also report an increase of the component's accretion and the absence of an accretion burst at the apastron, suggesting that the component's magnetic variation might be the cause of the inter-cycle variations of the system's accretion. We conclude on the presence of magnetospheric accretion for both systems, together with gravitational effects, especially for AK Sco, composed of more massive components.

#### 45. **On the growth and evolution of low-mass planets in pressure bumps**

Arnaud Pierens, Sean N. Raymond ★ Observations of protoplanetary discs have revealed dust rings which are likely due to the presence of pressure bumps in the disc. Because these structures tend to trap drifting pebbles, it has been proposed that pressure bumps may play an important role in the planet formation process. In this paper, we investigate the orbital evolution of a  $0.1 M_{\oplus}$  protoplanet embedded in a pressure bump using 2-dimensional hydrodynamical simulations of protoplanetary discs consisting of gas and pebbles. We examine the role of thermal forces generated by the pebble accretion-induced heat release, taking into account the feedback between luminosity

and eccentricity. We also study the effect of the pebble-scattered flow on the planet’s orbital evolution. Due to accumulation of pebbles at the pressure bump, the planet’s accretion luminosity is high enough to induce significant eccentricity growth through thermal forces. Accretion luminosity is also responsible for vortex formation at the planet position through baroclinic effects, which cause the planet escape from the dust ring if dust feedback onto the gas is neglected. Including the effect of the dust back-reaction leads to weaker vortices, which enable the planet to remain close to the pressure maximum on an eccentric orbit. Simulations in which the planet mass is allowed to increase as a consequence of pebble accretion resulted in the formation of giant planet cores with mass in the range  $5 - 20 M_{\oplus}$  over  $\sim 2 \times 10^4$  yrs. This occurs for moderate values of the Stokes number  $St \approx 0.01$  such that the pebble drift velocity is not too high and the dust ring mass not too small. Our results suggest that pressure bumps may be preferred locations for the formation of giant planets, but this requires a moderate level of grain growth within the disc.

#### 46. **Probing the physics of star formation (ProPStar): I. First resolved maps of the electron fraction and cosmic-ray ionization rate in NGC 1333**

Jaime E. Pineda, Olli Sipilä, Dominique M. Segura-Cox, Maria Teresa Valdivia-Mena, Roberto Neri, Michael Kuffmeier, Alexei V. Ivlev, Stella S. R. Offner, Maria Jose Maureira, Paola Caselli, Silvia Spezzano, Nichol Cunningham, Anika Schmiedeke, Mike Chen ★ Electron fraction and cosmic-ray ionization rates (CRIR) in star-forming regions are important quantities in astrochemical modeling and are critical to the degree of coupling between neutrals, ions, and electrons, which regulates the dynamics of the magnetic field. However, these are difficult quantities to estimate. We aim to derive the electron fraction and CRIR maps of an active star-forming region. We combined observations of the nearby NGC 1333 star-forming region carried out with the NOEMA interferometer and IRAM 30-m single dish to generate high spatial dynamic range maps of different molecular transitions. We used the  $\text{DCO}^+$  and  $\text{H}^{13}\text{CO}^+$  ratio (in addition to complementary data) to estimate the electron fraction and produce cosmic-ray ionization rate maps. We derived the first large-area electron fraction and CRIR resolved maps in a star-forming region, with typical values of  $10^{-6.5}$  and  $10^{-16.5} \text{ s}^{-1}$ , respectively. The maps present clear evidence of enhanced values around embedded young stellar objects (YSOs). This provides strong evidence for locally accelerated cosmic rays. We also found a strong enhancement toward the northwest region in the map that might be related either to an interaction with a bubble or to locally generated cosmic rays by YSOs. We used the typical electron fraction and derived a MHD turbulence dissipation scale of 0.054 pc, which could be tested with future observations. We found a higher cosmic-ray ionization rate compared to the canonical value for  $N(\text{H}_2) = 10^{21} - 10^{23} \text{ cm}^{-2}$  of  $10^{-17} \text{ s}^{-1}$  in the region, and it is likely generated by the accreting YSOs. The high value of the electron fraction suggests that new disks will form from gas in the ideal-MHD limit. This indicates that local enhancements of  $\zeta(\text{H}_2)$ , due to YSOs, should be taken into account in the analysis of clustered star formation.

#### 47. **Spectral characterization of young LT dwarfs**

L. Píscarreta, K. Mužić, V. Almendros-Abad, A. Scholz ★ We aim to provide a detailed characterization of near-infrared spectra for young LT brown dwarfs, including robust spectral typing, calibrating spectral indices, identifying possible binaries, and selecting suitable spectral standards. We processed and analyzed archival spectra from VLT/X-shooter for a sample of 56 dwarfs with ages between 10 and 600 Myr and spectral types between late-M and mid-T. We re-determine spectral types by comparing them with a set of literature templates and assess a large range of spectral indices, calibrated using a specifically designed literature sample. We are able to identify 15 spectral indices that are useful for spectral typing for specific spectral ranges discussed here and provide the scaling relations with spectral types. Moreover, we also identify 6 spectral indices which can be used to separate young L dwarfs from the field ones. The equivalent-widths of the alkali lines show a correlation with age, increasing towards the objects with higher surface gravity. From our sample, we confirm 3 that are likely to be binaries by their anomalous spectra that appear to be better fitted by a combination of spectral types. Finally, we identify 12 objects as preliminary near-infrared spectral standards for young LT dwarfs. This paper presents a significant step toward understanding the spectral sequence and properties of young L and T dwarfs. The relations and standards provided here will be useful for future spectroscopic work on young brown dwarfs and giant planets.

48. **Cracking the relation between mass and 1P-star fraction of globular clusters: I. Present-day cluster masses as a first tool**

Geneviève Parmentier ★ The phenomenon of multiple stellar populations is exacerbated in massive globular clusters, with the fraction of first-population (1P) stars a decreasing function of the cluster present-day mass. We decipher this relation in far greater detail than has been done so far. We assume (i) a fixed stellar mass threshold for the formation of second-population (2P) stars, (ii) a power-law scaling  $F_{1P} \propto m_{ecl}^{-1}$  between the mass  $m_{ecl}$  of newly-formed clusters and their 1P-star fraction  $F_{1P}$ , and (iii) a constant  $F_{1P}$  over time. The  $F_{1P}(m_{ecl})$  relation is then evolved up to an age of 12Gyr for tidal field strengths representative of the entire Galactic halo. The 12Gyr-old model tracks cover extremely well the present-day distribution of Galactic globular clusters in (mass,  $F_{1P}$ ) space. The distribution is curtailed on its top-right side by the scarcity of clusters at large Galactocentric distances, and on its bottom-left side by the initial scarcity of very high-mass clusters, and dynamical friction. Given their distinct dissolution rates, "inner" and "outer" model clusters are offset from each other, as observed. The locus of Magellanic Clouds clusters in (mass,  $F_{1P}$ ) space is as expected for intermediate-age clusters evolving in a gentle tidal field. Given the assumed constancy of  $F_{1P}$ , we conclude that 2P-stars do not necessarily form centrally-concentrated. We infer a minimum mass of  $4 \cdot 10^5 M_{\odot}$  for multiple-populations clusters at secular evolution onset. This high-mass threshold severely limits the amount of 2P-stars lost from evolving clusters, thereby fitting the low 2P-star fraction of the Galactic halo field.

49. **Introducing cuDisc: a 2D code for protoplanetary disc structure and evolution calculations**

Alfie Robinson, Richard A. Booth, James E. Owen ★ We present a new 2D axisymmetric code, cuDisc, for studying protoplanetary discs, focusing on the self-consistent calculation of dust dynamics, grain size distribution and disc temperature. Self-consistently studying these physical processes is essential for many disc problems, such as structure formation and dust removal, given that the processes heavily depend on one another. To follow the evolution over substantial fractions of the disc lifetime, cuDisc uses the CUDA language and libraries to speed up the code through GPU acceleration. cuDisc employs a second-order finite-volume Godunov solver for dust dynamics, solves the Smoluchowski equation for dust growth and calculates radiative transfer using a multi-frequency hybrid ray-tracing/flux-limited-diffusion method. We benchmark our code against current state-of-the-art codes. Through studying steady-state problems, we find that including 2D structure reveals that when collisions are important, the dust vertical structure appears to reach a diffusion-settling-coagulation equilibrium that can differ substantially from standard models that ignore coagulation. For low fragmentation velocities, we find an enhancement of intermediate-sized dust grains at heights of  $\sim 1$  gas scale height due to the variation in collision rates with height, and for large fragmentation velocities, we find an enhancement of small grains around the disc mid-plane due to collisional "sweeping" of small grains by large grains. These results could be important for the analysis of disc SEDs or scattered light images, given these observables are sensitive to the vertical grain distribution.

50. **DBNets: A publicly available deep learning tool to measure the masses of young planets in dusty protoplanetary discs**

Alessandro Ruzza, Giuseppe Lodato, Giovanni Pietro Rosotti ★ Current methods to characterize embedded planets in protoplanetary disc observations are severely limited either in their ability to fully account for the observed complex physics or in their computational and time costs. To address this shortcoming, we developed DBNets: a deep learning tool, based on convolutional neural networks, that analyses substructures observed in the dust continuum emission of protoplanetary discs to quickly infer the mass of allegedly embedded planets. We focussed on developing a method to reliably quantify not only the planet mass, but also the associated uncertainty introduced by our modelling and adopted techniques. Our tests gave promising results achieving an 87% reduction of the log Mp mean squared error with respect to an analytical formula fitted on the same data (DBNets metrics: lmse 0.016, r2-score 97%). With the goal of providing the final user of DBNets with all the tools needed to interpret their measurements and decide on their significance, we extensively tested our tool on out-of-distribution data. We found that DBNets can identify inputs strongly outside its training scope returning an uncertainty above a specific threshold and we thus provided a rejection criterion that helps determine the significance of the results obtained. Additionally, we outlined some limitations of our tool: it can be reliably applied only on discs observed with inclinations below approximately 60 deg, in the optically thin regime, with a resolution 8 times better than the gap radial location and with a signal-to-noise ratio higher than approximately ten. Finally, we applied DBNets to 33 actual observations of protoplanetary discs measuring the mass of 48 proposed planets and comparing our results with the available literature. We confirmed that most of the observed

gaps imply planets in the sub-Jupiter regime. DBNets is publicly available at [dbnets.fisica.unimi.it](http://dbnets.fisica.unimi.it).

## 51. Testing analytical methods to derive the cosmic-ray ionisation rate in cold regions via synthetic observations

E. Redaelli, S. Bovino, A. Lupi, T. Grassi, D. Gaete-Espinoza, G. Sabatini, P. Caselli ★ Cosmic rays (CRs) heavily impact the chemistry and physics of cold and dense star-forming regions. However, characterising their ionisation rate is still challenging from an observational point of view. In the past, a few analytical formulas have been proposed to infer the cosmic-ray ionization rate  $\zeta_2$  from molecular line observations. These have been derived from the chemical kinetics of the involved species, but they have not been validated using synthetic data processed with a standard observative pipeline. We aim to bridge this gap. We perform the radiative transfer on a set of three-dimensional magneto-hydrodynamical simulations of prestellar cores, exploring different initial  $\zeta_2$ , evolutionary stages, types of radiative transfer (e.g. assuming local-thermodynamic-equilibrium conditions), and telescope responses. We then compute the column densities of the involved tracers to determine  $\zeta_2$ , using, in particular, the equation proposed by Bovino et. al (2020) and by Caselli et al. (1998) both used nowadays. Our results confirm that the method of Bovino et al. (2020) accurately retrieves the actual  $\zeta_2$  within a factor of 2–3, in the physical conditions explored in our tests. Since we also explore a non-local thermodynamic equilibrium radiative transfer, this work indirectly offers insights into the excitation temperatures of common transitions at moderate volume densities ( $n \approx 10^5 \text{ cm}^{-3}$ ). We have also performed a few tests using the formula proposed by Caselli et al. (1998), which overestimates the actual  $\zeta_2$  by at least two orders of magnitudes. We also consider a new derivation of this method, which, however, still leads to large overestimates.

## 52. Predicting the Dominant Formation Mechanism of Multi-Planetary Systems

Cheyenne Shariat, Yasuhiro Hasegawa, Bradley M. S. Hansen, Tze Yeung Mathew Yu, Renyu Hu ★ Most, if not all, sun-like stars host one or more planets, making multi-planetary systems commonplace in our galaxy. We utilize hundreds of multi-planet simulations to explore the origin of such systems, focusing on their orbital architecture. The first set of simulations assumes in-situ assembly of planetary embryos, while the second explores planetary migration. After applying observational biases to the simulations, we compare them to 250+ observed multi-planetary systems, including 13 systems with planets in the habitable zone. For all of the systems, we calculate two of the so-called statistical measures: the mass concentration ( $S_c$ ) and orbital spacing ( $S_s$ ). After analytic and empirical analyses, we find that the measures are related to first-order with a power law:  $S_c \sim S_s^\beta$ . The in-situ systems exhibit steeper power-law relations relative to the migration systems. We show that different formation scenarios cover different regions in the  $S_s - S_c$  diagram with some overlap. Furthermore, we discover that observed systems with  $S_s < 30$  are likely dominated by the migration scenario, while those with  $S_s \geq 30$  are likely dominated by the in-situ scenario. We apply these criteria to determine that a majority (62%) of observed multi-planetary systems formed via migration, whereas most systems with currently observed habitable planets formed via in-situ assembly. This work provides methods of leveraging the statistical measures ( $S_s$  and  $S_c$ ) to disentangle the formation history of observed multi-planetary systems based on their present-day architectures.

## 53. A Statistical and Multiwavelength Photometric Analysis of a Young Embedded Open Star Cluster: IC 1590

A. H. Sheikh, Biman J. Medhi ★ We present a statistical and multiwavelength photometric studies of young open cluster IC 1590. We identified 91 cluster members using *Gaia* DR3 astrometry data using ensemble-based unsupervised machine learning techniques. From *Gaia* EDR3 data, we estimate the best-fitted parameters for IC 1590 using the Automated Stellar Cluster Analysis package (ASteCA) yielding the distance  $d \sim 2.87 \pm 0.02$  Kpc, age  $\sim 3.54 \pm 0.05$  Myr, metallicity  $z \sim 0.0212 \pm 0.003$ , binarity value of  $\sim 0.558$ , and extinction  $A_v \sim 1.252 \pm 0.4$  mag for an  $R_v$  value of  $\sim 3.322 \pm 0.23$ . We estimate the initial mass function slope of the cluster to be  $\alpha = 1.081 \pm 0.112$  for single stars and  $\alpha = 1.490 \pm 0.051$  for a binary fraction of  $\sim 0.558$  in the mass range  $1 M_\odot \leq m(M_\odot) \leq 100 M_\odot$ . The *G*-band luminosity function slope is estimated to be  $\sim 0.33 \pm 0.09$ . We use (*J* – *H*) versus (*H* – *K<sub>s</sub>*) color-color diagram to identify young stellar objects (YSOs). We found that all the identified YSOs have ages  $\leq 2$  Myr and masses  $\sim 0.35 - 5.5 M_\odot$ . We also fit the radial surface density profile. Using the galpy we performed orbit analysis of the cluster. The extinction map for the cluster region has been generated using the PNICER technique and it is almost similar to the dust structure obtained from the 500  $\mu\text{m}$  dust continuum emissions map of *Herschel* SPIRE. We finally at the end

discussed the star formation scenario in the cluster region.

#### 54. Planetesimal and planet formation in transient dust traps

Zs. Sándor, O. M. Guilera, Zs. Regály, W. Lyra ★ The ring-like structures in protoplanetary discs that are observed in the cold dust emission by ALMA, might be explained by dust aggregates trapped aerodynamically in pressure maxima. The effect of a transient pressure maximum is investigated that develops between two regimes with different turbulent levels. We study how such a pressure maximum collects dust aggregates and transforms them into large planetesimals and Moon-mass cores that can further grow to a few Earth-mass planets by pebble accretion, and eventually to giant planets, by considering the accretion of a gaseous envelope. A numerical model is developed, incorporating the evolution of gaseous disc, growth and transport of pebbles, N-body interactions of growing planetary cores and their backreaction to gas disc by opening a partial gap. Planetesimal formation by streaming instability is parametrized in our model. A transient pressure maximum efficiently accumulates dust particles that can grow larger than mm-size. If this happens, dust aggregates can be transformed by the streaming instability process into such large planetesimals, which can grow further by pebble accretion, according to our assumptions. As the gas evolves to its steady state, the pressure maximum vanishes, and the concentrated pebbles that are not transformed to planetesimals and accreted by the growing planet, drift inward. During this inward drift, if the conditions of the streaming instability are met, planetesimals are formed in a wide radial range of the disc. Conclusions. A transient pressure maximum is a favourable place for planetesimal and planet formation during its lifetime and the concentration of pebbles induces continuous formation of planetesimals even after its disappearance. Besides, the formation of a planet can trigger the formation of planetesimals over a wide area of the protoplanetary disc.

#### 55. Luminosity Outbursts in Interacting Protoplanetary Systems

Aleksandr M. Skliarevskii, Eduard I. Vorobyov ★ FU Orionis type objects (fuors) are characterized by rapid (tens to hundreds years) episodic outbursts, during which the luminosity increases by orders of magnitude. One of the possible causes of such events is a close encounter between stars and protoplanetary disks. Numerical simulations show that the fuor-like outburst ignition requires a very close encounter ranging from a few to a few tens of au. In contrast, the observed stellar objects in fuor binaries are usually hundreds of au apart. Simple mathematical estimates show that if such a close approach took place, the binary stellar components would have an unrealistic relative velocity, at least an order of magnitude greater than the observed velocity dispersion in young stellar clusters. Thus, the bursts are either triggered with a certain delay after passage of the periastron or their ignition does not necessary require a close encounter and hence the outburst is not caused by the primordial gravitational perturbation of the protoplanetary disk. In this work, an encounter of a star surrounded by a protoplanetary disk with a diskless external stellar object was modeled using numerical hydrodynamics simulations. We showed that even fly-bys with a relatively large periastron (at least 500 au) can result in fuor-like outbursts. Moreover, the delay between the periastron passage and the burst ignition can reach several kyr. It was shown for the first time by means of numerical modeling that the perturbation of the disk caused by the external object can trigger a cascade process, which includes the development of the thermal instability in the innermost disk followed by the magneto-rotational instability ignition. Because of the sequential development of these instabilities, the rapid increase in the accretion rate occurs, resulting in the luminosity increase by more than two orders of magnitude.

#### 56. PRODIGE – Planet-forming disks in Taurus with NOEMA. I. Overview and first results for $^{12}\text{CO}$ , $^{13}\text{CO}$ , and $\text{C}^{18}\text{O}$

D. Semenov, Th. Henning, S. Guilloteau, G. Smirnov-Pinchukov, A. Dutrey, E. Chapillon, V. Pietu, R. Franceschi, K. Schwarz, S. van Terwisga, L. Bouscasse, P. Caselli, C. Ceccarelli, N. Cunningham, A. Fuente, C. Gieser, T. -H. Hsieh, A. Lopez-Sepulcre, D. M. Segura-Cox, J. E. Pineda, M. J. Maureira, Th. Moeller, M. Tafalla, M. T. Valdivia-Mena ★ We are performing a line survey of 8 planet-forming Class II disks in Taurus with the IRAM Northern Extended Millimeter Array (NOEMA), as a part of the MPG-IRAM Observatory Program PRODIGE (PROtostars and DISks: Global Evolution; PIs: P. Caselli and Th. Henning). Compact and extended disks around T Tauri stars CI, CY, DG, DL, DM, DN, IQ Tau, and UZ Tau E are observed in 80 lines from  $>20$  C-, O-, N-, and S-bearing species. The observations in four spectral settings at 210-280 GHz with  $1\sigma$  rms sensitivity of 8-12 mJy/beam at  $0.9''$  and  $0.3$  km/s resolution will be completed in 2024. The uv-visibilitys are fitted with the DiskFit model to obtain key stellar and disk properties. In this paper, the combined  $^{12}\text{CO}$ ,  $^{13}\text{CO}$  and  $\text{C}^{18}\text{O}$   $J = 2 - 1$  data are

presented. We find that the CO fluxes and disk masses inferred from dust continuum tentatively correlate with the CO emission sizes. We constrain dynamical stellar masses, geometries, temperatures, the CO column densities and gas masses for each disk. The best-fit temperatures at 100 au are 17-37 K, and decrease radially with the power-law exponent  $q = 0.05-0.76$ . The inferred CO column densities decrease radially with the power-law exponent  $p = 0.2-3.1$ . The gas masses estimated from  $^{13}\text{CO}$  (2-1) are  $0.001 - 0.2 M_{\text{Sun}}$ . The best-fit CO column densities point to severe CO freeze-out in the disks. The DL Tau disk is an outlier, and has either stronger CO depletion or lower gas mass than the rest of the sample. The CO isotopologue ratios are roughly consistent with the observed values in disks and the low-mass star-forming regions.

## 57. Length and Velocity Scales in Protoplanetary Disk Turbulence

Debanjan Sengupta, Jeffrey N. Cuzzi, Orkan M. Umurhan, Wladimir Lyra ★ In the theory of protoplanetary disk turbulence, a widely adopted *ansatz*, or assumption, is that the turnover frequency of the largest turbulent eddy,  $\Omega_L$ , is the local Keplerian frequency  $\Omega_K$ . In terms of the standard dimensionless Shakura-Sunyaev  $\alpha$  parameter that quantifies turbulent viscosity or diffusivity, this assumption leads to characteristic length and velocity scales given respectively by  $\sqrt{\alpha}H$  and  $\sqrt{\alpha}c$ , in which  $H$  and  $c$  are the local gas scale height and sound speed. However, this assumption is not applicable in cases when turbulence is forced numerically or driven by some natural processes such as Vertical Shear Instability. Here we explore the more general case where  $\Omega_L \geq \Omega_K$  and show that under these conditions, the characteristic length and velocity scales are respectively  $\sqrt{\alpha/R'}H$  and  $\sqrt{\alpha R'}c$ , where  $R' \equiv \Omega_L/\Omega_K$  is twice the Rossby number. It follows that  $\alpha = \alpha t/R'$ , where  $\sqrt{\alpha t c}$  is the root-mean-square average of the turbulent velocities. Properly allowing for this effect naturally explains the reduced particle scale heights produced in shearing box simulations of particles in forced turbulence, and may help with interpreting recent edge-on disk observations; more general implications for observations are also presented. For  $R' > 1$  the effective particle Stokes numbers are increased, which has implications for particle collision dynamics and growth, as well as for planetesimal formation.

## 58. Small and Large Dust Cavities in Disks around mid-M Stars in Taurus

Yangfan Shi, Feng Long, Gregory J. Herczeg, Daniel Harsono, Yao Liu, Paola Pinilla, Enrico Ragusa, Doug Johnstone, Xue-Ning Bai, Ilaria Pascucci, Carlo F. Manara, Gijs D. Mulders, Lucas A. Cieza ★ High-angular resolution imaging by ALMA has revealed the near-universality and diversity of substructures in protoplanetary disks. However, disks around M-type pre-main-sequence stars are still poorly sampled, despite the prevalence of M-dwarfs in the galaxy. Here we present high-resolution (50 mas, 8 au) ALMA Band 6 observations of six disks around mid-M stars in Taurus. We detect dust continuum emission in all six disks, 12CO in five disks, and 13CO line in two disks. The size ratios between gas and dust disks range from 1.6 to 5.1. The ratio of about 5 for 2M0436 and 2M0450 indicates efficient dust radial drift. Four disks show rings and cavities and two disks are smooth. The cavity sizes occupy a wide range: 60 au for 2M0412, and 10 au for 2M0434, 2M0436 and 2M0508. Detailed visibility modeling indicates that small cavities of 1.7 and 5.7 au may hide in the two smooth disks 2M0450 and CIDA 12. We perform radiative transfer fitting of the infrared SEDs to constrain the cavity sizes, finding that micron-sized dust grains may have smaller cavities than millimeter grains. Planet-disk interactions are the preferred explanation to produce the large 60 au cavity, while other physics could be responsible for the three 10 au cavities under current observations and theories. Currently, disks around mid-to-late M stars in Taurus show a higher detection frequency of cavities than earlier type stars, although a more complete sample is needed to evaluate any dependence of substructure on stellar mass.

## 59. JWST Observations of Young protoStars (JOYS): Linked accretion and ejection in a Class I protobinary system

Łukasz Tychoniec, Martijn L. van Gelder, Ewine F. van Dishoeck, Logan Francis, Will R. M. Rocha, Alessio Caratti o Garatti, Henrik Beuther, Caroline Gieser, Kay Justtanont, Harold Linnartz, Valentin J. M. Le Gouellec, Giulia Perotti, Dev Rangaswamy, Benoît Tabone, Thomas P. Ray, Nashanty G. C. Brunken, Yuan Chen, Patrick J. Kavanagh, Pamela Klaassen, Katerina Slavicinska, Manuel Güdel, Goran Östlin ★ Accretion and ejection sets the outcome of the star and planet formation process. The mid-infrared wavelength range offers key tracers of those processes that were difficult to detect and spatially resolve in protostars until now. We aim to characterize the interplay between accretion and ejection in the low-mass Class I protobinary system TMC1, comprising two young stellar objects: TMC1-W and TMC1-E with 85 au separation. With the *James Webb* Space Telescope

(JWST) - Mid-Infrared Instrument (MIRI) observations in 5 - 28  $\mu\text{m}$  range, we measure intensities of emission lines of  $\text{H}_2$ , atoms and ions, e.g., [Fe II] and [Ne II], and HI recombination lines. We detect  $\text{H}_2$  outflow coming from TMC1-E, with no significant  $\text{H}_2$  emission from TMC1-W. The  $\text{H}_2$  emission from TMC1-E outflow appears narrow and extends to wider opening angles with decreasing  $E_{up}$  from S(8) to S(1) rotational transitions, indicating a disk wind origin. The outflow from TMC1-E protostar shows spatially extended emission lines of [Ne II], [Ne III], [Ar II], and [Ar III], with their line ratios consistent with UV radiation as a source of ionization. With ALMA, we detect accretion streamer infalling from  $> 1000$  au scales onto the TMC1-E component. TMC1-W protostar powers a collimated jet, detected with [Fe II] and [Ni II] consistent with energetic flow. A much weaker ionized jet is observed from TMC1-E. TMC1-W is associated with strong emission from hydrogen recombination lines, tracing the accretion onto the young star. Observations of a binary Class I protostellar system show that the two processes are clearly intertwined, with accretion from the envelope onto the disk influencing a wide-angle wind ejected on disk scales, while accretion from the protostellar disk onto the protostar is associated with the source launching a collimated high-velocity jet within the innermost regions of the disk.

## 60. **WTP 10aaaouw: Discovery of a new FU Ori outburst towards the RCW 49 star-forming region in NEOWISE data**

Vinh Tran, Kishalay De, Lynne Hillenbrand ★ Large-amplitude accretion outbursts in young stars are expected to play a central role in proto-stellar assembly. Outburst identification historically has taken place using optical techniques, but recent, systematic infrared searches are enabling their discovery in heavily dust-obscured regions of the Galactic plane. Here, we present the discovery of WTP 10aaaouw, a large-amplitude mid-infrared (MIR) outburst identified in a systematic search of NEOWISE data using new image subtraction techniques. The source is located towards the RCW 49 star-forming region, and estimated to be at a distance of  $\approx 4$  kpc via Gaia parallax measurement. Concurrent with the MIR brightening, the source underwent a  $\gtrsim 5$  mag outburst in the optical and near-infrared (NIR) bands, reaching a peak luminosity of  $\approx 260 L_\odot$  in 2014-2015, followed by a slow decline over the next 7 years. Analysis of the pre- and post-outburst spectral energy distributions reveal a pre-outburst stellar photosphere at a temperature of 3600 – 4000 K, surrounded by a likely two-component dust structure similar to a flat-spectrum or Class I type YSO. We present optical and NIR spectroscopy that show a GK-type spectrum in the optical bands exhibiting complex line profiles in strong absorption features, and evidence for a wind reaching a terminal velocity of  $\approx 400 \text{ km s}^{-1}$ . The NIR bands are characterized by a cooler M-type spectrum exhibiting a forest of atomic and molecular features. All together, the spectra demonstrate that WTP 10aaaouw is an FU Ori type outburst. Ongoing systematic infrared searches will continue to reveal the extent of this population in the Galactic disk.

## 61. **Curves of growth for transiting exocomets: Application to Fe II lines in the Beta Pictoris system**

T. Vignaud, A. Lecavelier des Etangs, F. Kiefer, A. -M. Lagrange, G. Hébrard, P. A. Strøm, A. Vidal-Madjar ★ This study introduces the exocomet curve of growth, a new method to analyse the variable absorptions observed in  $\beta$  Pictoris spectrum and link them to the physical properties of the transiting cometary tails. We show that the absorption depth of a comet in a set of lines arising from similar excitation levels of a given chemical species follows a simple curve as a function of the gf-values of the lines. This curve is the analogue of the curve of growth for interstellar absorption lines, where equivalent widths are replaced by absorption depths. To fit this exocomet curve of growth, we introduce a model where the cometary absorption is produced by a homogeneous cloud, covering a limited fraction of the stellar disc. This model is defined by two parameters:  $\alpha$ , the covering factor of the cloud, and  $\beta$ , related to its typical optical depth. This model is tested on two comets observed with the Hubble Space Telescope in December 1997 and October 2018, in a set of Fe II lines at 275 nm. The measured absorption depths are found to satisfactorily match the two-parameter curve of growth model, indicating that both comets cover roughly 40 unity. Then, we show that if we consider a set of lines arising from a wider range of energy levels, the absorbing species seems to be populated at thermodynamical equilibrium, causing the cometary absorption to follow a curve of growth as a function of  $gf \cdot e^{-E_l/k_B T}$  (where T is the temperature of the absorbing medium). For the comet observed on December 6, 1997, we derive a temperature of  $10500 \pm 500$  K and a total Fe II column density of  $(1.11 \pm 0.09) \times 10^{15} \text{ cm}^{-2}$ . By probing the population of the highest excited energy levels ( $E_l \sim 25000 \text{ cm}^{-1}$ ), we also estimate an electronic density of  $(3 \pm 1) \times 10^7 \text{ cm}^{-3}$ .

## 62. Magnetic fields in the Southern Coalsack and beyond

M. J. F. Versteeg, Y. Angarita, A. M. Magalhães, M. Haverkorn, C. V. Rodrigues, R. Santos-Lima, Koji S. Kawabata ★ Starlight polarimetry, when combined with accurate distance measurements, allows for exploration of the three-dimensional structure of local magnetic fields in great detail. We present optical polarimetric observations of stars in and close to the Southern Coalsack, taken from the Interstellar Polarization Survey (IPS). Located in five fields of view approximately  $0.3^\circ$  by  $0.3^\circ$  in size, these data represent the highest density of optical polarimetric observations in the Southern Coalsack to date. Using these data, combined with accurate distances and extinctions based on Gaia data, we are able to characterize the magnetic field of the Coalsack and disentangle contributions to the polarization caused by the Southern Coalsack and a background structure. For the Southern Coalsack, we find an average magnetic field orientation of  $\theta \sim 75^\circ$  with respect to the Galactic north pole and an average plane-of-sky magnetic field strength of approximately  $B_{POS} = 10 \mu G$ , using the Davis-Chandrasekhar-Fermi (DCF) method. These values are in agreement with some earlier estimates of the Coalsack’s magnetic field. In order to study the distant structure, we introduce a simple method to separate and isolate the polarization of distant stars from foreground contribution. For the distant structure, which we estimate to be located at a distance of approximately 1.3-1.5 kpc, we find an average magnetic field orientation of  $\theta \sim 100^\circ$  and we estimate a field strength of  $B_{POS} \sim 10 \mu G$ , although this will remain highly uncertain until the precise nature of the distant structure can be uncovered.

## 63. The interplay between forming planets and photoevaporating discs II: Wind-driven gas redistribution

Michael L. Weber, Giovanni Picogna, Barbara Ercolano ★ Disc winds and planet-disc interactions are two crucial mechanisms that define the structure, evolution and dispersal of protoplanetary discs. While winds are capable of removing material from discs, eventually leading to their dispersal, massive planets can shape their disc by creating sub-structures such as gaps and spiral arms. We study the interplay between an X-ray photoevaporative disc wind and the substructures generated due to planet-disc interactions to determine how their mutual interactions affect the disc’s and the planet’s evolution. We perform three-dimensional hydrodynamic simulations of viscous ( $\alpha = 6.9 \cdot 10^{-4}$ ) discs that host a Jupiter-like planet and undergo X-ray photoevaporation. We trace the gas flows within the disc and wind and measure the accretion rate onto the planet, as well as the gravitational torque that is acting on it. Our results show that the planetary gap takes away the wind’s pressure support, allowing wind material to fall back into the gap. This opens new pathways for material from the inner disc (and part of the outer disc) to be redistributed through the wind towards the gap. Consequently, the gap becomes shallower, and the flow of mass across the gap in both directions is significantly increased, as well as the planet’s mass-accretion rate (by factors  $\approx 5$  and  $\approx 2$ , respectively). Moreover, the wind-driven redistribution results in a denser inner disc and less dense outer disc, which, combined with the recycling of a significant portion of the inner wind, leads to longer lifetimes of the inner disc, contrary to the expectation in a planet-induced photoevaporation (PIPE) scenario that has been proposed in the past.

## 64. Disk Wind Feedback from High-mass Protostars. III. Synthetic CO Line Emission

Duo Xu, Jonathan C. Tan, Jan E. Staff, Jon P. Ramsey, Yichen Zhang, Kei E. Tanaka ★ To test theoretical models of massive star formation it is important to compare their predictions with observed systems. To this end, we conduct CO molecular line radiative transfer post-processing of 3D magneto-hydrodynamic (MHD) simulations of various stages in the evolutionary sequence of a massive protostellar core, including its infall envelope and disk wind outflow. Synthetic position-position-velocity (PPV) cubes of various transitions of CO,  $^{13}\text{CO}$ , and  $\text{C}^{18}\text{O}$  emission are generated. We also carry out simulated Atacama Large Millimeter/submillimeter Array (ALMA) observations of this emission. We compare the mass, momentum and kinetic energy estimates obtained from molecular lines to the true values, finding that the mass and momentum estimates can have uncertainties of up to a factor of four. However, the kinetic energy estimated from molecular lines is more significantly underestimated. Additionally, we compare the mass outflow rate and momentum outflow rate obtained from the synthetic spectra with the true values. Finally, we compare the synthetic spectra with real examples of ALMA-observed protostars and determine the best fitting protostellar masses and outflow inclination angles. We then calculate the mass outflow rate and momentum outflow rate for these sources, finding that both rates agree with theoretical protostellar evolutionary tracks.

**65. Dense Core Collisions in Molecular Clouds: Formation of Streamers and Binary Stars**

Yuta Yano, Fumitaka Nakamura, Shinichi W. Kinoshita ★ Dense core collisions, previously regarded as minor in star formation, are proposed to play a significant role in structure formation around protostellar envelopes and binary formation. Using archival data of nearby star-forming regions, we determine the frequencies of core collisions. Our calculations reveal that a typical core is likely to undergo multiple interactions with other cores throughout its lifetime. To further investigate the core collision process, we employ adaptive mesh refinement hydrodynamic simulations with sink particles. Our simulations demonstrate that following the formation of a protostar within a gravitationally-unstable core, the merging core's accreting gas gives rise to a rotationally-supported circumstellar disk. Meanwhile, the region compressed by the shock between the cores develops into asymmetric arms that connect with the disk. Gas along these arms tends to migrate inward, ultimately falling toward the protostar. One of the arms, a remnant of the shock-compressed region, dominates over the second core gas, potentially exhibiting a distinct chemical composition. This is consistent with recent findings of large-scale streamers around protostars. Additionally, we found that collisions with velocities of  $\sim 1.5 \text{ km s}^{-1}$  result in the formation of a binary system, as evidenced by the emergence of a sink particle within the dense section of the shocked layer. Overall, dense core collisions are highlighted as a critical process in creating  $10^3$  au-scale streamers around protostellar systems and binary stars.

**66. Turbulent vortex with moderate dust settling probed by scattering-induced polarization in the IRS 48 system**

Haifeng Yang, Manuel Fernández-López, Zhi-Yun Li, Ian W. Stephens, Leslie W. Looney, Zhe-Yu Daniel Lin, Rachel Harrison ★ We investigate the crescent-shaped dust trap in the transition disk, Oph IRS 48, using well-resolved (sub)millimeter polarimetric observations at ALMA Band 7 ( $870 \mu\text{m}$ ). The dust polarization map reveals patterns consistent with dust scattering-induced polarization. There is a relative displacement between the polarized flux and the total flux, which holds the key to understanding the dust scale heights in this system. We model the polarization observations, focusing on the effects of dust scale heights. We find that the interplay between the inclination-induced polarization and the polarization arising from radiation anisotropy in the crescent determines the observed polarization; the anisotropy is controlled by the dust optical depth along the midplane, which is, in turn, determined by the dust scale height in the vertical direction. We find that the dust grains can neither be completely settled nor well mixed with the gas. The completely settled case produces little radial displacement between the total and polarized flux, while the well-mixed case produces an azimuthal pattern in the outer (radial) edge of the crescent that is not observed. Our best model has a gas-to-dust scale height ratio of 2, and can reproduce both the radial displacement and the azimuthal displacement between the total and polarized flux. We infer an effective turbulence  $\alpha$  parameter of approximately  $0.0001 - 0.005$ . The scattering-induced polarization provides insight into a turbulent vortex with a moderate level of dust settling in the IRS 48 system, which is hard to achieve otherwise.

**67. Gas content and evolution of a sample of YSO associations at  $d \lesssim 3.5$  kpc from the Sun**

Ji-Xuan Zhou, Guang-Xing Li, Bing-Qiu Chen ★ Young Stellar Objects (YSO) are newly formed stars from molecular clouds. They stay close to where they were born and serve as good tracers to study gas and star formation. During cloud evolution, young massive stars can disrupt the surrounding gas through stellar feedback, changing the gas distribution. We study the distribution of the gas around a sample of YSO associations located at  $d \lesssim 3.5$  kpc from the Sun by comparing the location and morphology between  $^{12}\text{CO}$  ( $J = 1-0$ ) emission, Planck  $870 \mu\text{m}$  maps and YSO associations. Based on the spatial distribution of the gas compared to that of the YSOs, we classify the YSO associations into six types: direct, close, bubble, complex, diffuse, and clean associations. The complex associations are large structures consisting of both gas-rich and gas-poor segments. We study the velocity dispersion-size relation toward different association types. From the ratio between different types, we estimate a feedback time of  $\approx 1.7$  Myr in the solar neighborhood. The sample sets a solid foundation to explore the relationship between interstellar medium evolution, star formation, and Galaxy structure.

68. **Effects of physical conditions on the stellar initial mass function: The low-metallicity star-forming region Sh 2-209**

Marie Zinnkann, Henriette Wirth, Pavel Kroupa ★ Recent work suggested that the variation of the initial mass function (IMF) of stars depends on the physical conditions, notably, the metallicity and gas density. We investigated the properties of two clusters, namely the main cluster (MC) and the subcluster (SC), in the low-metallicity HII region Sh 2-209 (S209) based on recently derived IMFs. We tested three previously published correlations using previous observations: the top-heaviness of the IMF in dependence on metallicity, the half-mass radius, and the most massive star in dependence on the stellar mass of the embedded clusters. For this region, two different galactocentric distances, namely 10.5 kpc and 18 kpc, were considered, where an age-distance-degeneracy was found for the previously determined IMF to be consistent with other formulated metallicity and density dependent IMFs. The determined half-mass radius ( $0.080 \pm 0.005$ ) pc and the embedded cluster density ( $0.2 \pm 0.1$ )  $10^6$  Msun pc $^{-3}$  for the MC with an age of 0.5 Myr in S209 assuming a galactocentric distance of 18 kpc support the assumption that a low-metallicity environment results in a denser cluster, which leads to a top-heavy IMF. Thus, all three tests are consistent with the previously published correlations. The results for S209 are placed in the context with the IMF determination within the metal-poor cluster in the star-forming region NGC 346 in the Small Magellanic Cloud.

69. **Multi-band reflectance and shadowing of RX J1604.3-2130 protoplanetary disk in scattered light**

Huisheng Zhong, Bin B. Ren, Bo Ma, Chen Xie, Jie Ma, Nicole L. Wallack, Dimitri Mawet, Garreth Ruane ★ Context. Spatially-resolved circumstellar disk spectrum and composition can provide valuable insights into the bulk composition of forming planets, as well as the mineralogical signatures that emerge during and after planet formation. Aims. We aim to systemically extract the RX J1604.3-213010 (J1604 hereafter) protoplanetary disk in high-contrast imaging observations, and obtain its multi-band reflectance in visible to near-infrared wavelengths. Methods. We obtained coronagraphic observations of J1604 from the Keck Observatory's NIRC2 instrument, and archival data from the Very Large Telescope's SPHERE instrument. Using archival images to remove star light and speckles, we recovered the J1604 disk and obtained its surface brightness using forward modeling. Together with polarization data, we obtained the relative reflectance of the disk in  $R$ ,  $J$ ,  $H$  ( $H2$  and  $H3$ ),  $K$  ( $K1$  and  $K2$ ), and  $L'$  bands spanning two years. Results. Relative to the J1604 star, the resolved disk has a reflectance of  $\sim 10^{-1}$  arcsec $^{-2}$  in  $R$  through  $H$  bands and  $\sim 10^{-2}$  arcsec $^{-2}$  in  $K$  and  $L'$  bands, showing a blue color. Together with other systems, we summarized the multi-band reflectance for 9 systems. We also identified varying disk geometry structure, and a shadow that vanished between June and August in 2015. Conclusions. Motivated by broad-band observations, the deployment of cutting-edge technologies could yield higher-resolution reflection spectra, thereby informing the dust composition of disks in scattered light in the future. With multi-epoch observations, variable shadows have the potential to deepen insights into the dynamic characteristics of inner disk regions.